The Mechanisms of Fluxionality of $[Fe_3(CO)_{12-n}\{P(OR)_3\}_n]$ (R = Me, n = 0—3; R = Pr^i, n = 2 or 3) and the X-Ray Structure of $[Fe_3(CO)_{10}\{P(OMe)_3\}_2]$ †

Harry Adams, Neil A. Bailey,* Gary W. Bentley, and Brian E. Mann*
Department of Chemistry, The University, Sheffield S3 7HF

The solution structures of the major isomers of $[Fe_3(CO)_{10}\{P(OMe)_3\}_2]$ and $[Fe_3(CO)_9\{P(OMe)_3\}_3]$ have been unambiguously established in solution. Probable structures of $[Fe_3(CO)_{11}\{P(OMe)_3\}]$, the minor isomers of $[Fe_3(CO)_{10}\{P(OMe)_3\}_2]$ and $[Fe_3(CO)_9\{P(OMe)_3\}_3]$, and the major isomer of $[Fe_3(CO)_9\{P(OPr^i)_3\}_3]$ in solution are proposed. The solution structures of $[Fe_3(CO)_{12}]$ and $[Fe_3(CO)_{11}\{P(OMe)_3\}]$ are discussed. It is shown that there is a very-low-energy dynamic process which is apparent in the carbonyl positions of the crystal structure of $[Fe_3(CO)_{12}]$. In addition, there are three, and probably four, higher-energy dynamic processes which have been established from ^{13}C and ^{31}P n.m.r. investigations. The implications of the low-energy dynamic process in the solid-state ^{13}C n.m.r. spectrum are discussed. The X-ray structure of $[Fe_3(CO)_{10}\{P(OMe)_3\}_2]$ shows it to have the $P(OMe)_3$ ligands forming an approximately linear P–Fe–Fe–P arrangement, with bridging carbonyls between the unique unsubstituted iron and a substituted iron. Disorder prevented an accurate structure determination.

The structure of tri-iron dodecacarbonyl has presented problems for chemists since its discovery in 1906.[1] It has had a long history of erroneous structures and these have been reviewed.[2] In 1930, Hieber and Becker[3] used freezing-point depression measurements in $[Fe(CO)_5]$ to show that it is trimeric. This work was followed by a long period of confusion. I.r.[4–8] and Mössbauer[9–11] spectroscopic investigations were used to study the structure, but this work caused more confusion. The first strong clues to the structure of $[Fe_3(CO)_{12}]$ came from the X-ray structures of $[Fe_3H(CO)_{11}]^-$,[12] $[Fe_3(CO)_{11}(PPh_3)]$,[13] and $[Os_3(CO)_{12}]$.[14] It was not until the X-ray structure of $[Fe_3(CO)_{12}]$ was determined that the *solid-state* structure was unambiguously established as (**1**; L^1 = L^2 = CO).[2,15,16]

The solution structure of $[Fe_3(CO)_{12}]$ still remains to be established. The i.r. spectrum of $[Fe_3(CO)_{12}]$ in solution shows two strong, well defined, bands in the terminal stretching region and two weak bands in the bridging carbonyl stretching region.[4–8] It was suggested that these weak bands are not fundamentals, but overtones and/or combinations.[6,7] Subsequently, evidence was presented that these vibrations are fundamentals.[8] The i.r. spectra could be interpreted in terms of either a bridged structure in solution, as is found in the X-ray structure in the solid state, or in terms of a fully bridge-opened species, similar to that found for $[Ru_3(CO)_{12}]$[17] and $[Os_3(CO)_{12}]$.[14] The i.r. spectrum of $[Fe_3(CO)_{12}]$ in an argon matrix at 20 K is consistent with the bridged solid-state structure.[18] It was concluded that the structures of $[Fe_3(CO)_{12}]$ in solution and matrix are different. A more recent i.r. study led to the conclusion that $[Fe_3(CO)_{12}]$ in solution is a mixture of bridged and unbridged species.[19] Very recently, it has been concluded from an extended X-ray absorption fine structure (EXAFS) study that $[Fe_3(CO)_{12}]$ adopts primarily an all-terminal carbonyl co-ordination in light petroleum solution, but there is a substantial population of bridging sites in frozen CH_2Cl_2 solution.[20]

The ^{13}C n.m.r. spectrum of $[Fe_3(CO)_{12}]$ provides little assistance in the determination of its solution structure, giving a singlet down to −150 °C.[21] It was concluded that there is a very-low-energy dynamic process with an activation energy of less than 6 kcal mol^{-1}. It was postulated that exchange occurs *via* the merry-go-round mechanism,[21] see Scheme 1. Further confusion arises from the solid-state ^{13}C n.m.r. spectrum, which consists of six signals in the ratio 1:1:1:1:1:1 at 31 °C,[22] but these signals changed on cooling to −90 °C.[23] The solid-state n.m.r. spectrum was interpreted in terms of two different molecules in the unit cell being interconverted by rotation of the Fe_3 triangle.

When a molecule fails to yield limiting low-temperature ^{13}C n.m.r. spectra, the usual approach is to introduce substituents to block dynamic pathways, and so to obtain limiting low-temperature n.m.r. spectra. This has been attempted by Johnson and co-workers[24] and Farrar and Lunniss.[25] Johnson and co-workers[24] synthesized a number of monosubstituted derivatives, $[Fe_3(CO)_{11}L]$, (**1**; L^1 = PMe_2Ph or $P(OR)_3$; R = Et, Pr^i, or Ph; L^2 = CO). They observed that at low temperature each compound gave rise to three ^{13}CO n.m.r. signals, in the intensity ratio, 6:4:1. On warming, two signals exchange to give at room temperature two signals in the ratio 10:1. They rationalized these observations in terms of an icosahedron ⟷ cube octahedron ⟷ icosahedron rearrangement giving rise to the Cotton merry-go-round exchange of six carbonyls, see Scheme 1, and a trigonal twist at the unsubstituted bridge iron atom. These two mechanisms give rise to the low-temperature 6:4:1 pattern, but require that the activation energy for the two dynamic processes is less than about 6 kcal mol^{-1}. This is possible for the merry-go-round mechanism, but is improbable for the trigonal twist.

Farrar and Lunniss[25] synthesized $[Fe_3(CO)_{10}\{P(OMe)_3\}_2]$ and $[Fe_3(CO)_{10}\{P(OMe)_3\}\{P(OPh)_3\}]$. In the low-temperature ^{13}C n.m.r. spectrum of $[Fe_3(CO)_{10}\{P(OMe)_3\}_2]$, they observed seven carbonyl signals in the ratio 1.4:2:6:2.8:2.8:1:1, and the ^{31}P n.m.r. spectrum showed the presence of two isomers in the ratio 2:1.4. It was concluded that the structures of the two isomers are [**1**; L^1 = L^2 = $P(OMe)_3$] or (**2**) and (**3**). The minor isomer was believed to be (**3**), having signals at δ 251.2, 214.3, and 212.3 p.p.m. in the intensity ratio 2:4:4. There is a rapid

† 1,2;1,2-Di-μ-carbonyl-1,1,1,2,2,3,3,3-octacarbonyl-1,3-bis(trimethyl phosphite)-*triangulo*-tri-iron.

Supplementary data available: see Instructions for Authors, *J. Chem. Soc., Dalton Trans.*, 1989, Issue 1, pp. xvii—xx.
Non-S.I. unit employed: cal = 4.184 J.

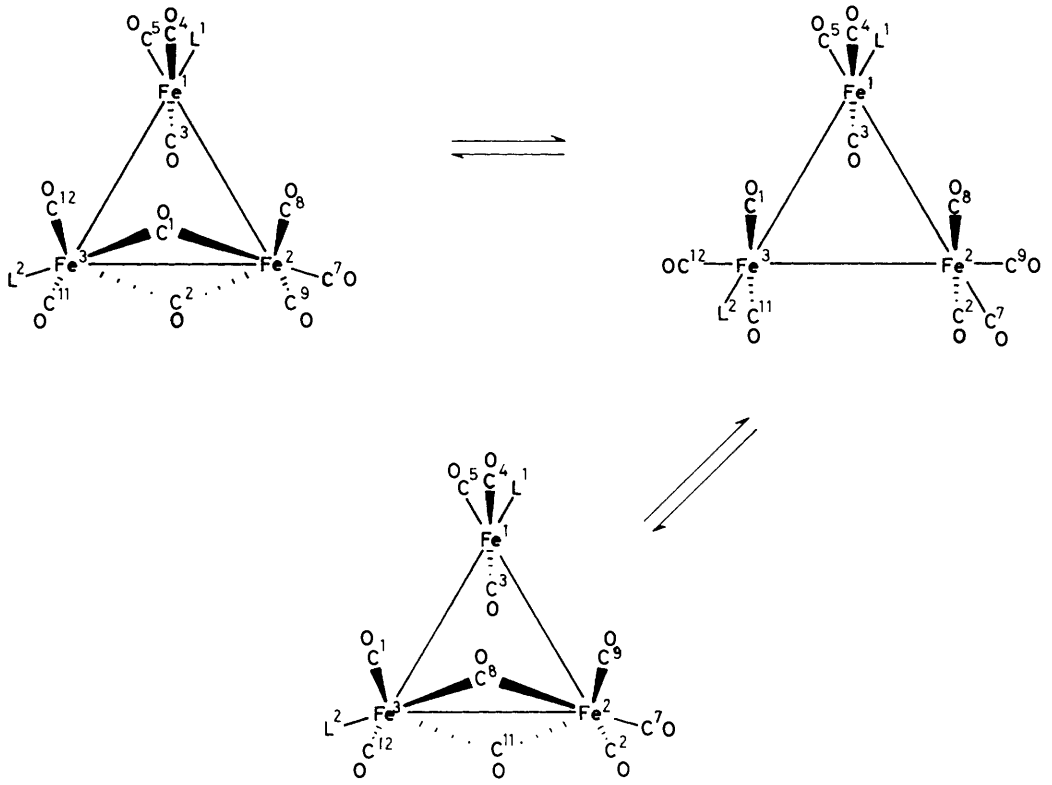

Scheme 1. The Cotton merry-go-round mechanism [21]

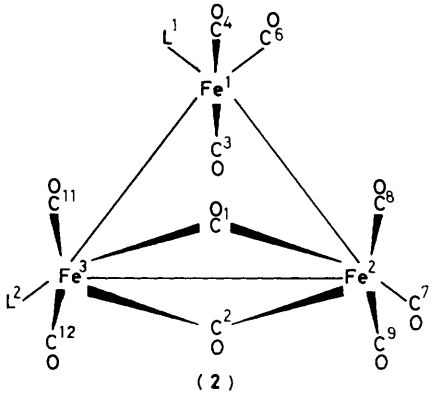

(2)

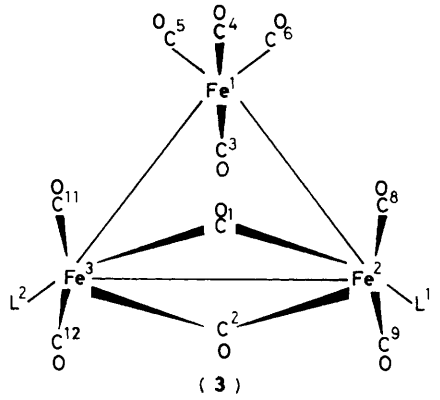

(3)

trigonal twist at the unsubstituted iron atom at −80 °C, making carbonyls C^3O, C^4O, C^5O, and C^6O equivalent, despite this generally being a slower process. This is in contrast to Johnson's conclusion that the rapid trigonal twist occurs at a bridge iron atom. On warming to −60 °C, all these carbonyls exchange by an unidentified mechanism. At −80 °C, the second isomer has signals at δ 221.5, 220.9, 209.5, and 202.4 p.p.m., in the intensity ratio 2:6:1:1. The signal of intensity 6 was attributed to rapid exchange by the merry-go-round mechanism. It was not discussed why the merry-go-round mechanism is very low energy in [**1**; L^1 = $P(OMe)_3$, L^2 = CO] and [**1**; L^1 = L^2 = $P(OMe)_3$], but could be stopped in (**3**). At −20 °C, exchange of the two inequivalent $P(OMe)_3$ ligands occurs, coupled with exchange of the signal of intensity 6 with that of intensity 2. At higher temperature there is interconversion of the two isomers. Farrar also noted that $[Fe_3(CO)_9\{P(OMe)_3\}_3]$ gives rise to one isomer with three ^{31}P n.m.r. signals.

It is clear that there is considerable confusion in these n.m.r. observations, and it is impossible to rationalize them. For example, it is postulated that, at *ca.* −100 °C, the merry-go-round mechanism is fast in $[Fe_3(CO)_{11}\{P(OMe)_3\}]$ and one isomer of $[Fe_3(CO)_{10}\{P(OMe)_3\}_2]$, but is slow in the other isomer. We have therefore reinvestigated the problem.

Results and Discussion

The Very-low-energy Carbonyl-exchange Mechanism: Concerted Bridge Opening and Closing.—The key to the solution of the dynamics of $[Fe_3(CO)_{12}]$ and its derivatives has been in the literature since Cotton determined the reliable structure in 1974.[16] Burgi and Dunitz [26] showed that *X*-ray structures can be used to identify low-energy dynamic pathways. Recently, it has been shown for $[Rh_6C(CO)_{13}]^{2-}$ that there is a good correlation between the shape of the thermal ellipsoids of the carbonyls and the dynamic pathway of carbonyl scrambling.[27] Using the published atomic positions, the non-bonded Fe···CO distances for $[Fe_3(CO)_{12}]$ have been calculated, see Table 1. Calculations have been performed

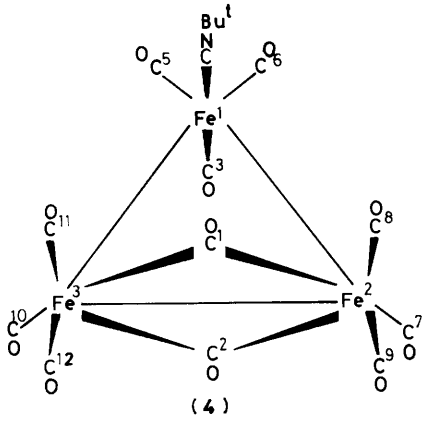

(4)

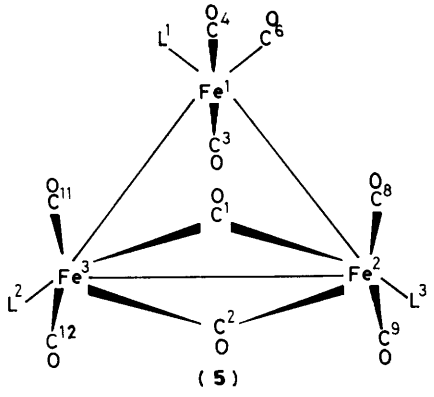

(5)

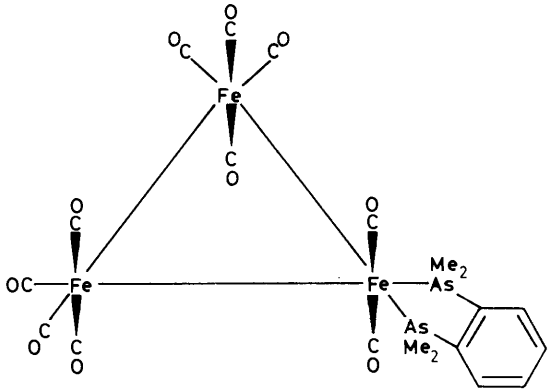

(6)

Table 1. Selected Fe–CO distances, in Å, in $[Fe_3(CO)_{12}]$, $[Fe_3(CO)_{11}(PPh_3)]$, both isomers, $[Fe_3(CO)_{11}(CNBu^t)]$, and $[Fe_3(CO)_9(PMe_2Ph)_3]$

(*a*) $[Fe_3(CO)_{12}]$[16]					
Fe^1–C^8	3.10	Fe^2–C^1	2.11	Fe^3–C^1	1.96
Fe^1–C^9	3.31	Fe^2–C^2	1.93	Fe^3–C^2	2.21
Fe^1–C^{11}	3.18	Fe^2–C^3	3.07	Fe^3–C^3	3.19
Fe^1–C^{12}	3.27	Fe^2–C^4	3.24	Fe^3–C^4	3.19
(*b*) $[Fe_3(CO)_{11}(PPh_3)]$ [**1**; L^1 = CO, L^2 = PPh_3][13]					
Fe^1–C^8	3.08	Fe^2–C^1	2.03	Fe^3–C^1	1.85
Fe^1–C^9	3.20	Fe^2–C^2	1.90	Fe^3–C^2	1.98
Fe^1–C^{11}	3.11	Fe^2–C^3	3.07	Fe^3–C^3	3.03
Fe^1–C^{12}	3.12	Fe^2–C^4	3.10	Fe^3–C^4	3.24
(*c*) $[Fe_3(CO)_{11}(PPh_3)]$ [**1**; L^1 = PPh_3, L^2 = CO][13]					
Fe^1–C^8	3.07	Fe^2–C^1	2.04	Fe^3–C^1	1.86
Fe^1–C^9	3.28	Fe^2–C^2	1.86	Fe^3–C^2	2.08
Fe^1–C^{11}	3.20	Fe^2–C^3	2.96	Fe^3–C^3	3.06
Fe^1–C^{12}	3.23	Fe^2–C^4	3.17	Fe^3–C^4	3.15
(*d*) $[Fe_3(CO)_{11}(CNBu^t)]$[28]					
Fe^1–C^8	2.97	Fe^2–C^1	2.01	Fe^3–C^1	2.02
Fe^1–C^9	3.32	Fe^2–C^2	2.04	Fe^3–C^2	2.02
Fe^1–C^{11}	3.10	Fe^2–C^3	3.07	Fe^3–C^3	3.11
Fe^1–C^{12}	3.21	Fe^2–L^4*	3.33	Fe^3–L^4*	3.33
(*e*) $[Fe_3(CO)_9(PMe_2Ph)_3]$[29]					
Fe^1–C^8	3.04	Fe^2–C^1	2.04	Fe^3–C^1	1.97
Fe^1–C^9	3.19	Fe^2–C^2	1.97	Fe^3–C^2	2.01
Fe^1–C^{11}	3.19	Fe^2–C^3	3.03	Fe^3–C^3	3.12
Fe^1–C^{12}	3.14	Fe^2–C^4	3.16	Fe^3–C^4	3.21

* L^4 refers to the isonitrile carbon of the $CNBu^t$ ligand.

for related published data on $[Fe_3(CO)_{11}(PPh_3)]$,[13] $[Fe_3(CO)_{11}(CNBu^t)]$, (**4**),[28] and $[Fe_3(CO)_9(PMe_2Ph)_3]$, (**5**).[29] In the case of $[Fe_3(CO)_{11}(PPh_3)]$ there are two isomers present in the one crystal structure, and the calculations have been performed for both isomers. The data for $[Fe_3(CO)_{11}(PPh_3)]$ are poor, but this may simply reflect the disorder in the crystal. An examination of the data shows that the relative bond lengths are Fe^2–C^2 < Fe^2–C^1, Fe^3–C^1 < Fe^3–C^2, Fe^1–C^8 < Fe^1–C^9, and Fe^2–C^3 < Fe^2–C^4. There is a concerted lean of C^3O towards Fe^2 and C^8O towards Fe^1. There are concomitant movements of the carbonyls on Fe^2 towards the geometry found in the *X*-ray structure of $[Fe_3(CO)_{10}\{1,2\text{-}(Me_2As)_2C_6H_4\}]$, (**6**).[30] This carbonyl movement provides a mechanism for carbonyl exchange, see Scheme 2, with concerted bridge formation on the Fe^1–Fe^2 bond as the bridge opens on the Fe^2–Fe^3 bond. When L^1 = L^2 this mechanism causes pairwise equivalence of carbonyls $C^1O \longleftrightarrow C^3O$, $C^2O \longleftrightarrow C^8O$, $C^4O \longleftrightarrow C^{11}O$, $C^5O \longleftrightarrow C^{12}O$, $C^6O \longleftrightarrow C^{10}O$, and $C^7O \longleftrightarrow C^9O$, but does not move the carbonyls from the iron atoms with which they are associated. A second process is required to produce the solution ^{13}C n.m.r. spectra observed at −100 °C. This process generates an apparent plane of symmetry through the plane of the iron triangle, causing equivalence of carbonyls $C^1O \longleftrightarrow C^2O$, $C^3O \longleftrightarrow C^4O$, $C^8O \longleftrightarrow C^9O$, and $C^{11}O \longleftrightarrow C^{12}O$, see Scheme 3. When these two dynamic processes are combined they produce a cyclic pathway exchanging $C^7O \longleftrightarrow C^8O \longleftrightarrow C^1O \longleftrightarrow C^{12}O \longleftrightarrow C^{11}O$ and also $C^4O \longleftrightarrow C^5O \longleftrightarrow C^3O \longleftrightarrow C^9O \longleftrightarrow C^8O$, see Scheme 4. It is proposed that both these mechanisms require very low activation energies, <6 kcal mol^{-1}, as proposed by Cotton and Hunter.[21] It is proposed that this is the dynamic process that cannot be frozen out on the n.m.r. time-scale, and that all other carbonyl-exchange processes are relatively slow at −100 °C. It is then possible to account for the low-temperature ^{13}C n.m.r. spectra of $[Fe_3(CO)_{12-n}\{P(OR)_3\}_n]$ (R = Me, *n* = 1—3; R = Pr^i, *n* = 2).

The Solution ^{13}C N.M.R. Spectra at ca. −100 °C.—$[Fe_3(CO)_{12}]$. In the case of $[Fe_3(CO)_{12}]$ the dynamic process in Scheme 4 would cause the carbonyls to collapse to a ratio of 10:2 if it is restricted to one pair of Fe–Fe edges. A series of exchanges involving different pairs of Fe–Fe edges results in complete scrambling of all the carbonyls. This gives rise to one ^{13}C n.m.r. signal as is observed down to −160 °C. The

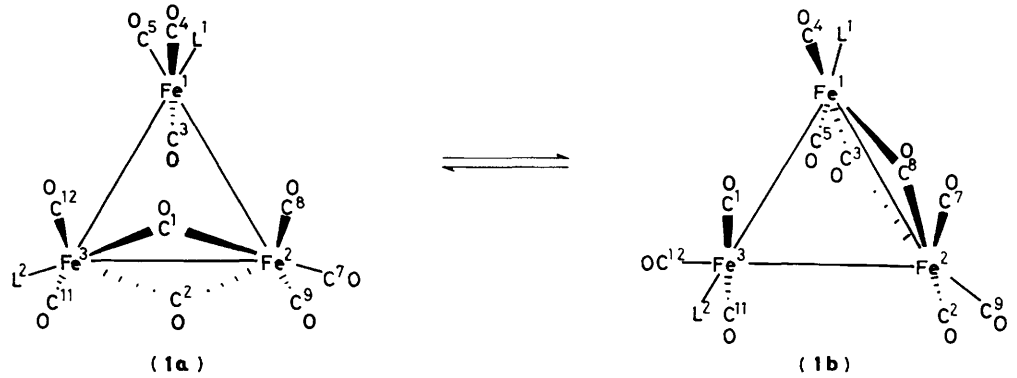

Scheme 2. The proposed very-low-energy exchange pathway for carbonyl exchange in $[Fe_3(CO)_{12}]$ ($L^1 = L^2 = CO$), $[Fe_3(CO)_{11}\{P(OMe)_3\}]$ [$L^1 = P(OMe)_3$, $L^2 = CO$], and of $[Fe_3(CO)_{10}\{P(OR)_3\}_2]$ [$L^1 = L^2 = P(OR)_3$, R = Me or Pr^i], isomer (**1**)

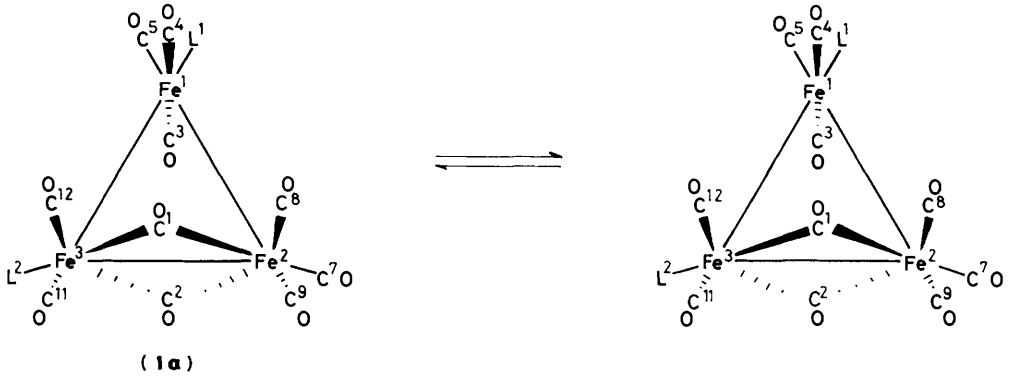

Scheme 3. The proposed low-energy exchange pathway for $[Fe_3(CO)_{12}]$ ($L^1 = L^2 = CO$), $[Fe_3(CO)_{11}\{P(OMe)_3\}]$ [$L = P(OMe)_3$, $L^2 = CO$], and $[Fe_3(CO)_{10}\{P(OR)_3\}_2]$[$L^1 = L^2 = P(OR)_3$, R = Me or Pr^i], isomer (**1**)

mechanism in Scheme 2 also accounts for the solid-state ^{13}C n.m.r. spectrum at −93 °C (see below).

$[Fe_3(CO)_{11}L]$. For $[Fe_3(CO)_{11}L]$ there are two isomers with equatorial L, (**1a**) and (**1b**), $L^1 = L$, $L^2 = CO$, as found in the *X*-ray structure of $[Fe_3(CO)_{11}(PPh_3)]$.[13] The possibility of a structure with axial phosphorus ligands is improbable. Many *X*-ray structures have been published for $[M_3(CO)_{12-n}L_n]$ (M = Fe, Ru, or Os; L = phosphorus ligand).[13,29–32] In all cases the phosphorus ligand is equatorial. An axial phosphorus ligand is only observed for $[Ru_3(CO)_9\{(Bu^n_2P)_3SiMe\}]$ where ligand constraints enforce this.[33] Studies of the fluxional mechanisms of $[Os_3(CO)_{12-n}L_n]$ (L = phosphorus ligand) have found no evidence for mechanisms involving axial phosphorus ligands.[34] The compound $[Fe_3(CO)_{10}\{1,2\text{-}(Me_2As)_2C_6H_4\}]$ could adopt a structure with bridging carbonyls and an axial arsenic ligand, but the *X*-ray structure shows that it has semi-bridging carbonyls with equatorial arsenic ligands, (**6**).[30]

In $[Fe_3(CO)_{11}\{P(OMe)_3\}]$, the presence of the $P(OMe)_3$ ligand labels each edge as being different. The mechanism in Scheme 2 interconverts the two isomers, (**1a**) and (**1b**), $L^1 = CO$, $L^2 = P(OMe)_3$. This dynamic process, combined with that in Scheme 3, exchanges carbonyls $\overleftrightarrow{C^7O \longleftrightarrow C^2O \longleftrightarrow C^1O \longleftrightarrow C^{12}O \longleftrightarrow C^{11}O}$ and $\overleftrightarrow{C^4O \longleftrightarrow C^5O \longleftrightarrow C^3O \longleftrightarrow C^9O \longleftrightarrow C^8O}$, resulting in three signals in the ratio 5:5:1, one, an averaged signal arising from C^1O, C^2O, C^7O, $C^{11}O$, and $C^{12}O$, a second, an averaged signal arising from C^3O, C^4O, C^5O, C^8O, and C^9O, and the third unique signal being from $L^1 = CO$. According to Johnson and co-workers, the intensity ratio is 6:4:1. The compound $[Fe_3(CO)_{11}\{P(OMe)_3\}]$ was synthesized according to the literature method,[35] and the ^{13}C n.m.r. spectrum measured at − 101 °C in CD_2Cl_2, see Figure 1. Care was taken to obtain an accurate integral. The spectrum was recorded without ^1H decoupling to avoid nuclear Overhauser effect (n.O.e.) errors in the integral. The T_1 values were determined, and the ^{13}C n.m.r. spectrum was recorded with $5T_1$ between pulses.* The integration clearly shows three signals at δ 219.1 [$J(^{31}P\text{–}^{13}C)$ = 13 Hz], 216.0, and 202.8 p.p.m. in the intensity ratio 5:5:1, rather than the published 6:4:1, consistent with the mechanism in Scheme 4. The observation of ^{31}P coupling with the signal at δ 219.1 p.p.m. is consistent with it being due to the averaged signal from carbonyls C^1O, C^2O, C^7O, $C^{11}O$, and $C^{12}O$. The remaining carbonyls do not approach the $P(OMe)_3$ ligand. The signal at δ 202.8 p.p.m. is assigned to $L^2 = CO$.

$[Fe_3(CO)_{10}L_2]$. There are three possible structures for $[Fe_3(CO)_{10}L_2]$ with equatorial phosphorus ligands (**1**; $L^1 = L^2 = L$), (**2**), and (**3**). Structures with axial phosphorus ligands are omitted as these are not found in *X*-ray structures. As previously reported,[25] the ^{31}P n.m.r. spectrum of $[Fe_3(CO)_{10}\{P(OMe)_3\}_2]$ shows the presence of two isomers in the temperature-dependent ratio of *ca.* 1:0.7. One isomer gives rise to only one ^{31}P n.m.r. signal at δ 162.4 p.p.m., even at −95 °C. According to Farrar and Lunniss,[25] this is isomer (**3**),

* T_1 was determined approximately using the inversion recovery pulse sequence as 0.28 ± 0.08, 0.204 ± 0.006, and 0.172 ± 0.006 s, for the signals at δ 219.4, 216.3, and 203.0 p.p.m. respectively. A delay of 2.0 s was used between the 90° pulses to ensure complete relaxation, and hence accurate integrals. The actual integrals obtained were 5.00 (taken as reference):4.95:1.01.

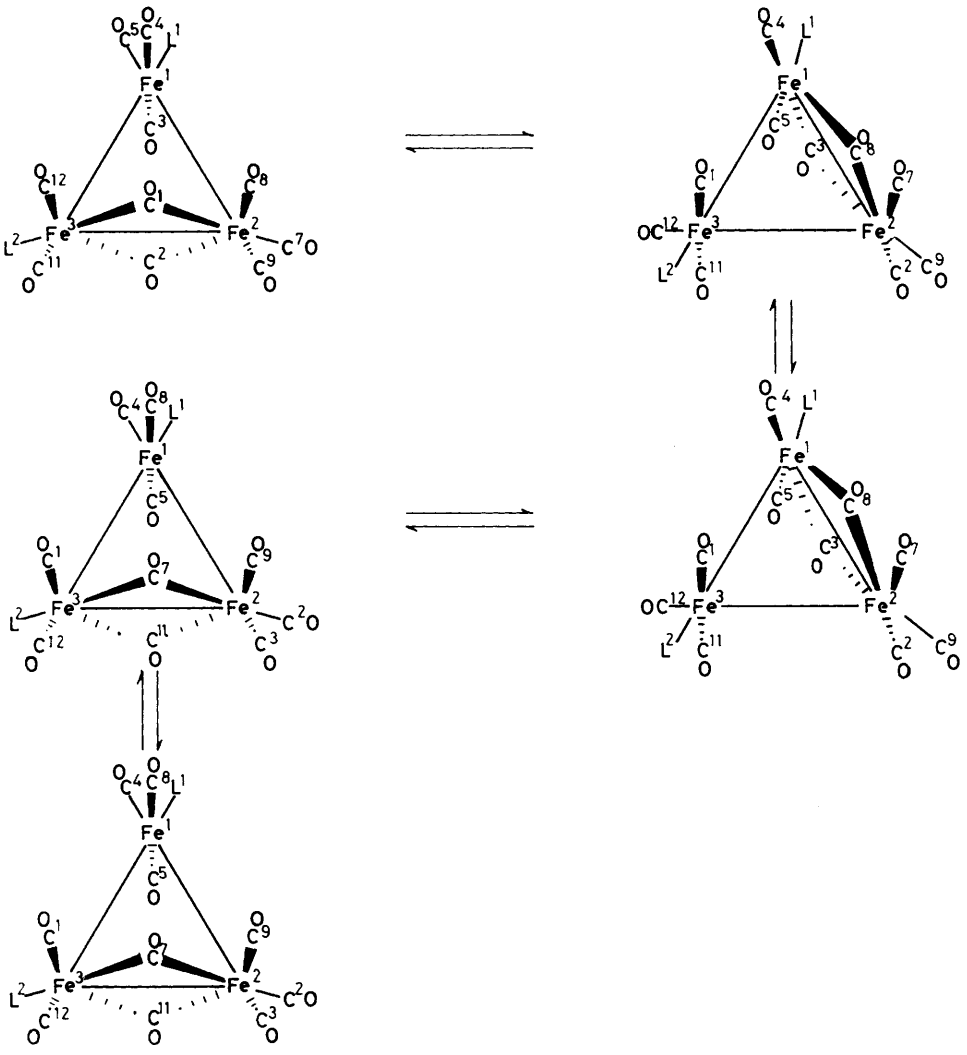

Scheme 4. The combined low-energy exchange pathway for $[Fe_3(CO)_{12}]$ ($L^1 = L^2 = CO$), $[Fe_3(CO)_{11}\{P(OMe)_3\}]$ [$L^1 = P(OMe)_3$, $L^2 = CO$], and $[Fe_3(CO)_{10}\{P(OR)_3\}_2]$ [$L^1 = L^2 = P(OR)_3$, R = Me or Pr^i], isomer (**1**)

while the other isomer is (**2**) which gives two ^{31}P n.m.r. signals at δ 156.7 and 167.4 p.p.m. Farrar dismissed the presence of isomer [**1**; $L^1 = L^2 = P(OMe)_3$]. It is this isomer which crystallizes from methanol and the *X*-ray structure was determined, see below. This does not prove, but strongly suggests, that isomer [**1**; $L^1 = L^2 = P(OMe)_3$] is present in solution. Farrar assigned the signal at δ 253.3 p.p.m. to the bridging carbonyls in isomer (**3**). If this assignment is correct, this signal should be a triplet, coupling to the two equivalent $^{31}P(OMe)_3$ groups. Experiment shows that this signal is a doublet, $J(^{31}P-^{13}C) = 13$ Hz due to coupling to only *one* $^{31}P(OMe)_3$ group. This is consistent with this signal arising from the bridging carbonyls in structure (**1**) or (**2**).

Compound [**1**; $L^1 = L^2 = P(OMe)_3$] undergoes the dynamic process shown in Scheme 4. This fully exchanges L^1 and L^2, and the carbonyls produce two sets of carbonyls in the ratio 5:5. Due to the symmetry of the complex, these two sets of carbonyls have the same chemical shift, and only one signal results. By analogy with $[Fe_3(CO)_{11}\{P(OMe)_3\}]$, each set of signals couples with only *one* phosphite ligand. Carbonyls C^1O, C^2O, C^7O, $C^{11}O$, and $C^{12}O$ are associated with the $P(OMe)_3$ in position L^2, and C^3O, C^4O, C^5O, C^8O, and C^9O are associated with the $P(OMe)_3$ in position L^1. The mechanism does not permit complete scrambling of the carbonyls. Consequently, the resulting averaged signal is a *doublet*. This is exactly the behaviour observed in the n.m.r. spectra at low temperature with a doublet being observed at δ 221.9 p.p.m. in the ^{13}C n.m.r. spectrum.

The second isomer shows two ^{31}P n.m.r. signals at δ 156.7 and 167.4 p.p.m. Isomers (**2**) and (**3**) cannot undergo the fluxional process in Scheme 2 and will give a limiting low-temperature spectrum at −100 °C. Isomer (**2**) should give rise to six ^{13}C signals in the ratio 2:2:2:2:1:1 and two ^{31}P signals, while isomer (**3**) should give rise to four ^{13}C signals in the ratio 2:4:2:2 and one ^{31}P signal. The ^{13}C n.m.r. spectrum at −100 °C shows six signals, in addition to the doublet due to [**1**; $L^1 = L^2 = P(OMe)_3$].

The intensities of the published ^{13}C n.m.r. spectrum[25] of $[Fe_3(CO)_{10}\{P(OMe)_3\}_2]$ are inconsistent with these conclusions. The spectrum was remeasured in CD_2Cl_2 at −92 °C, and is shown in Figure 2. Farrar reported that the signals are in the intensity ratio 1.4:2:6:2.8:2.8:1:1,[25] but integration of the

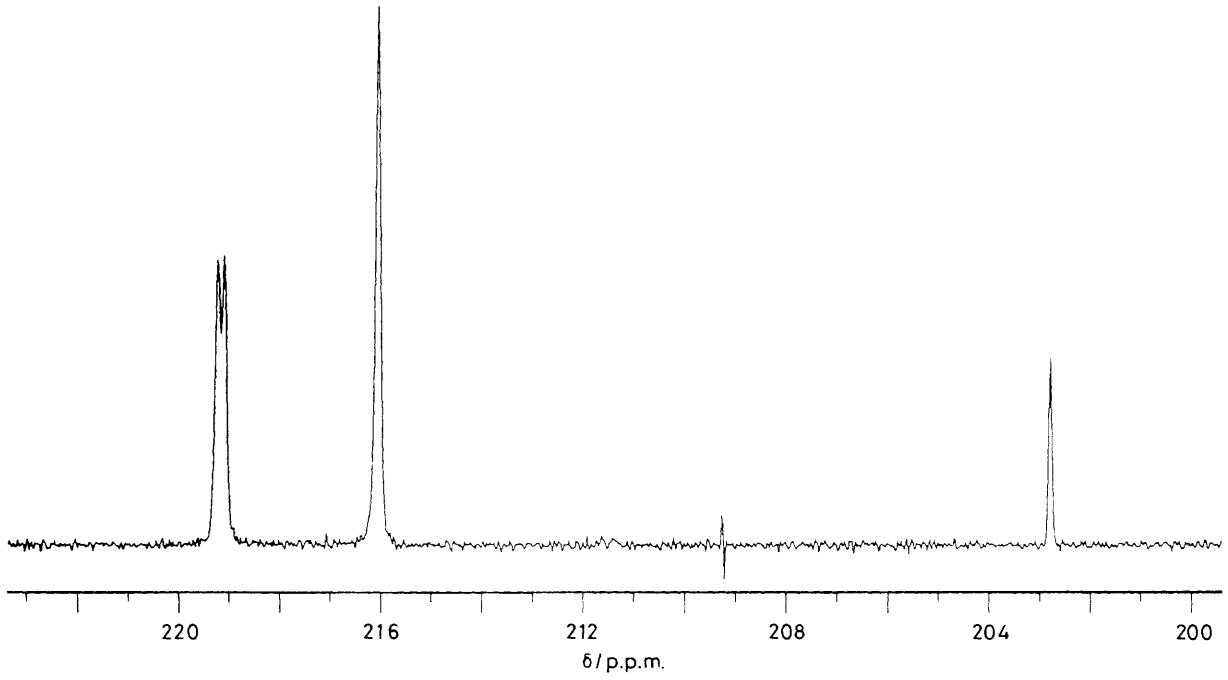

Figure 1. The 100.62-MHz ^{13}C n.m.r. spectrum of the carbonyl ligands of $[Fe_3(CO)_{11}\{P(OMe)_3\}]$ at −101 °C in CD_2Cl_2

spectrum in Figure 2 gives the ratio 2:2:6.5:2:2:1:1.* The separation of the signals at δ 222.1 and 221.9 p.p.m. is poor at −92 °C, but at −60 °C these signals separate, permitting more reliable integration of the signal at δ 222.1 p.p.m. against those at 221.9, 210.4, and 203.3 p.p.m., the signals at δ 252.3, 215.1, and 213.5 p.p.m. being extremely broadened by exchange. The chemical shift of the signal at δ 252.3 p.p.m. is typical of a bridging carbonyl.[39] The weakness of this signal in Farrar's report[25] may be due to the longer relaxation time of bridging carbonyls.[36–38] This ^{13}C n.m.r. spectrum shows a signal at δ 221.9 p.p.m. which is a doublet under high resolution, with $J(^{31}P-^{13}C)$ = 13 Hz. This signal is assignable to isomer [**1**; $L^1 = L^2 = P(OMe)_3$]. The remaining signals are at δ 252.3 [$J(^{31}P-^{13}C)$ = 13], 222.1 [$J(^{31}P-^{13}C)$ = 33], 215.1 [$J(^{31}P-^{13}C)$ = 15], 213.5, 210.4 [$J(^{31}P-^{13}C)$ = 7 Hz], and 203.3 p.p.m., in the ratio 2:2:2:2:1 consistent with the limiting ^{13}C spectrum expected for (**2**). The ^{13}C n.m.r. spectrum gives the ratio of isomers as 1:0.65 in agreement with the ^{31}P n.m.r. spectrum. The ^{13}C n.m.r. signals may be assigned as C^1, C^2 at δ 252.3, C^3, C^4 at 222.1, C^{11}, C^{12} at 215.1, C^8, C^9 at 213.5, C^6 at 210.4, and C^7 at 203.3 p.p.m. These assignments are significantly different from those given earlier by Farrar and Lunniss.[25] The signals assigned for isomer (**2**) can be used to predict the averaged signal for [**1**; $L^1 = L^2 = P(OMe)_3$], at δ 221.8 p.p.m. with $J(^{31}P-^{13}C)$ = 10 Hz. The chemical shift is in excellent agreement with experiment. The coupling constant is somewhat low, but this will in part be due to contributions from unresolved coupling in (**2**).

As a further check on the structures of the two isomers of $[Fe_3(CO)_{10}\{P(OMe)_3\}_2]$, $[Fe_3(CO)_{10}\{P(OPr^i)_3\}_2]$ was synthesized. The ^{31}P n.m.r. spectrum at −35 °C showed three signals at δ 160.2, 155.1, and 149.5 p.p.m. in the intensity ratio 1:2.9:1. There are only relatively small changes in the isomer ratio from 1:0.76 to 1:1.45 with the increasing steric size of the phosphite ligand from $P(OMe)_3$ to $P(OPr^i)_3$. This is consistent with the two ligands being well separated, as in [**1**; $L^1 = L^2 = P(OR)_3$, R = Me or Pr^i] and (**2**). It would be anticipated that structure (**3**) would be strongly disfavoured by bulky ligands. A marked ligand steric effect is observed in $[Fe_3(CO)_9\{P(OPr^i)_3\}_3]$, where in one isomer, (**5**), there are two bulky ligands close together, as in (**3**), see below. Considerable difficulties were encountered in obtaining a limiting low-temperature ^{13}C spectrum of $[Fe_3(CO)_{10}\{P(OPr^i)_3\}_2]$. Although the compounds are very soluble in CD_2Cl_2 at room temperature, they crystallize out on cooling to −90 °C. The ^{31}P n.m.r. spectrum shows that when this crystallization occurs, the signal due to isomer [**1**; $L^1 = L^2 = P(OPr^i)_3$] diminishes, presumably because it is this isomer that crystallizes, and the interconversion of isomers is slow at this temperature. A ^{13}C n.m.r. spectrum was obtained by adjusting the concentration and rapid cooling to −90 °C to slow crystallization, but the signal:noise ratio was poor, leading to a poor integral.† The spectrum was similar to that found for $[Fe_3(CO)_{10}\{P(OMe)_3\}_2]$, see Table 2, but with signal intensites of approximately 2:2:15:2:2:1:1, giving a ratio of isomers of 1:1.5 in good agreement with the ^{31}P n.m.r. data.

$[Fe_3(CO)_9L_3]$. There are only two possible structures for $[Fe_3(CO)_9\{P(OMe)_3\}_3]$ with equatorial phosphorus ligands, (**5**) and (**7**). As the mechanism in Scheme 2 is blocked by the $P(OMe)_3$ ligands, (**5**) should be static on the n.m.r. time-scale at −90 °C, to give five ^{13}CO n.m.r. signals in the ratio 2:2:2:2:1. Isomer (**7**) cannot give a simple bridged structure without putting a $P(OMe)_3$ ligand into an axial position. This type of arrangement is only observed when ligand constraints permit no alternative. The ^{31}P n.m.r. spectrum showed the presence of

* T_1 was determined approximately using the inversion recovery pulse sequence as 0.27 ± 0.04 s for C^1O and C^2O, and 0.13 to 0.19 ± 0.04 s for the terminal carbonyls and the averaged signal for [**1**; $L^1 = L^2 = P(OMe)_3$]. These short relaxation times arise from the dominance of chemical shift anisotropy relaxation at 9.4 T, and the long tumbling time of this large molecule at −92 °C.[36–38] A delay of 2.0 s was used between 90° pulses to ensure complete relaxation and hence accurate integrals. The actual integrals obtained were 2.00 (taken as reference):8.49 {(**2**; C^3O, C^4O) and [**1**: $L^1 = L^2 = P(OMe)_3$]}:1.93:1.86:0.99:1.01.

† Due to experimental difficulties, these integrals are subject to error. The actual intensities obtained were 2.0 (reference):2.2:15.6:2.0:2.3:1.3:1.2.

Table 2. The ^{13}C chemical shifts (p.p.m.) of $[Fe_3(CO)_{12-n}\{P(OR)_3\}_n]$ [R = Me, n = 1—3; R = Pr^i, n = 2], with $J(^{31}P-^{13}C)$, in Hz, in parentheses

n	Structure	R	C^1O, C^2O	C^3O, C^4O	C^8O, C^9O	$C^{11}O, C^{12}O$	C^6O, C^7O	$C^{10}O$
1	(1)	Me				202.8		
2	(2)	Me	252.3	222.1	213.5	215.1	210.4	203.3
			(13)	(33)	(15)	(7)		
2	(2)	Pr^i	251.0	222.2	213.2	214.8	210.4	203.3
			(13)	(31)	(15)	*a*		
3	(4)	Me	252.4	221.4	215.8[b]	215.6[b]	211.3	
			a	(30)	(19)	(19)		

[a] Broad due to unresolved coupling. [b] Relative assignment unknown.

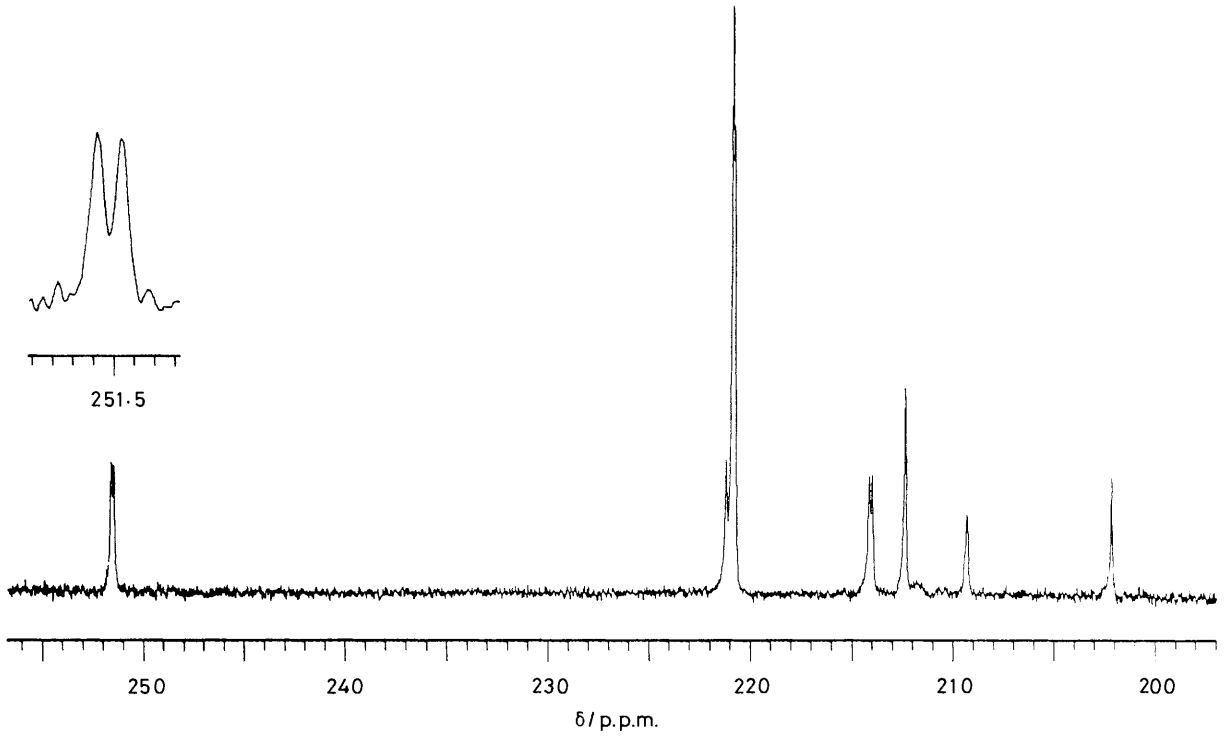

Figure 2. The 100.62-MHz ^{13}C n.m.r. spectrum of the carbonyl ligands of $[Fe_3(CO)_{10}\{P(OMe)_3\}_2]$ at −92 °C in CD_2Cl_2

two isomers, with signals at δ 160.9, 162.9, 167.6, and 170.9 p.p.m. in the ratio 1:1:0.7:1 at −50 °C and below, rather than one species as reported by Farrar and Lunniss.[25] The ^{31}P n.m.r. spectrum is also consistent with the major species being (**5**) and the minor species being (**7**) in a ratio of 1:0.23. The ^{13}C n.m.r. spectrum is consistent with structure (**5**) for the major isomer with signals at δ 253.4 (C^1, C^2), 221.4 [$J(^{31}P-^{13}C)$ = 30, C^3, C^4], 215.8 [$J(^{31}P-^{13}C)$ = 19], 215.6 [$J(^{31}P-^{13}C)$ = 19 Hz, C^8, C^9, C^{11}, C^{12}], and 211.3 p.p.m. (C^7). The minor isomer has signals at δ 230.7, 228.9, and 210.6 p.p.m. in the approximate ratio 3:3:3, see Figure 3. The signals due to the minor isomer were weak and ill defined. Grant and Manning[40] had previously noted that for $[Fe_3(CO)_9\{P(OPr^i)_3\}_3]$ the i.r. spectrum showed that the concentration of the bridged isomer was very low. This compound was synthesized and the ^{31}P n.m.r. spectrum at −70 °C showed four signals at δ 156.4, 157.8, 163.0, and 166.2 p.p.m. in the ratio 1.00:1.00:65:1.00. The repulsion between the two adjacent $P(OPr^i)_3$ ligands in (**5**) causes this isomer to be destabilized, and the symmetric isomer, (**7**), to be stabilized by *ca.* 2 kcal mol^{-1}. This large change in isomer ratio can be compared with the small change observed on ligand replacement in $[Fe_3(CO)_{10}\{P(OR)_3\}_2]$ (R = Me or Pr^i), where the ligands are well separated. This provides further

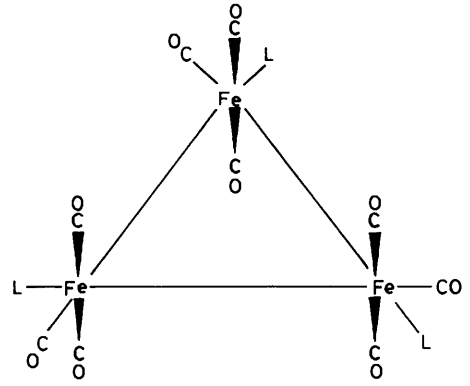

(**7**)

evidence that (**3**) is not one of the observed isomers of $[Fe_3(CO)_{10}\{P(OMe)_3\}_2]$. The ^{13}C n.m.r. spectrum of $[Fe_3(CO)_9\{P(OPr^i)_3\}_3]$ shows three signals in the ratio 3:3:3 at δ 231.3 [$J(^{31}P-^{13}C)$ = 25], 227.8 [$J(^{31}P-^{13}C)$ = 25 Hz],

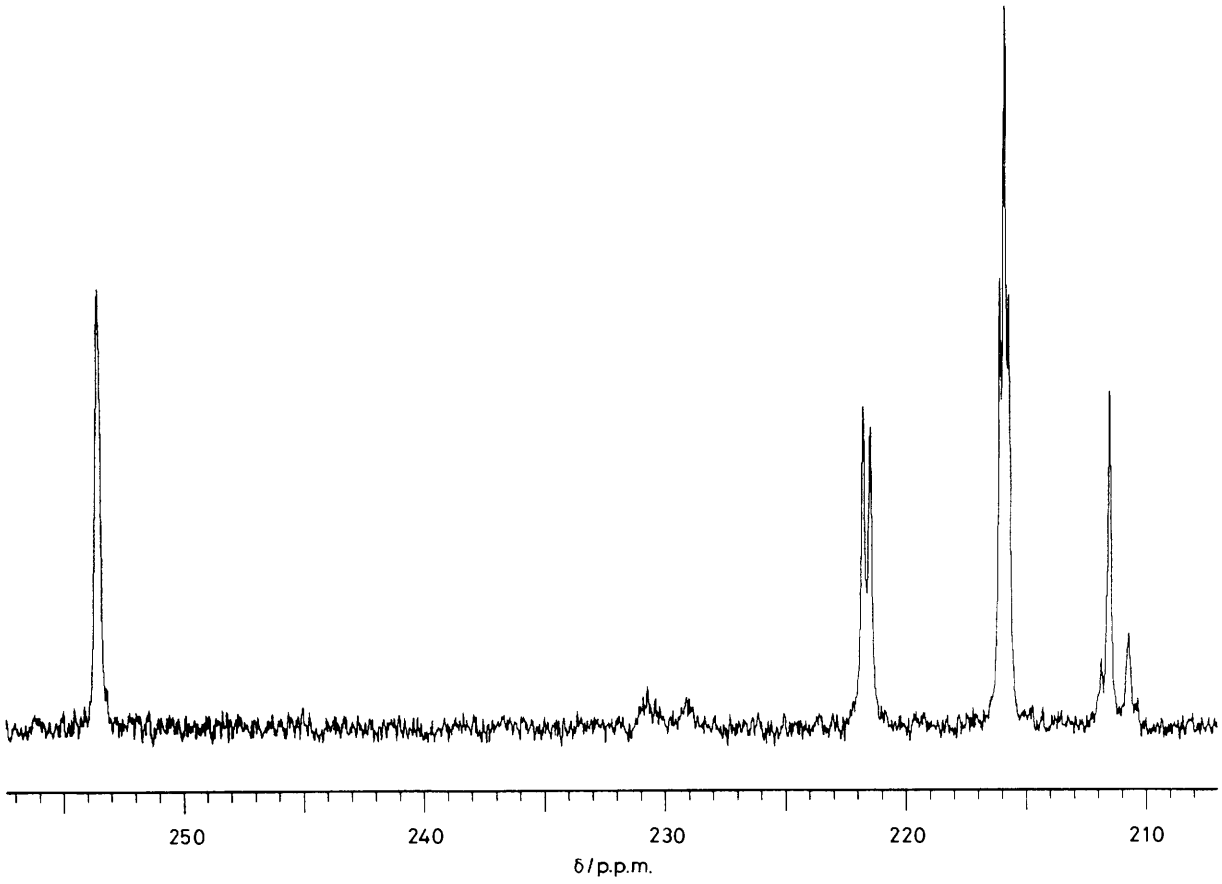

Figure 3. The 100.62-MHz ^{13}C n.m.r. spectrum of the carbonyl ligands of $[Fe_3(CO)_9\{P(OMe)_3\}_3]$ at -80 °C in CD_2Cl_2

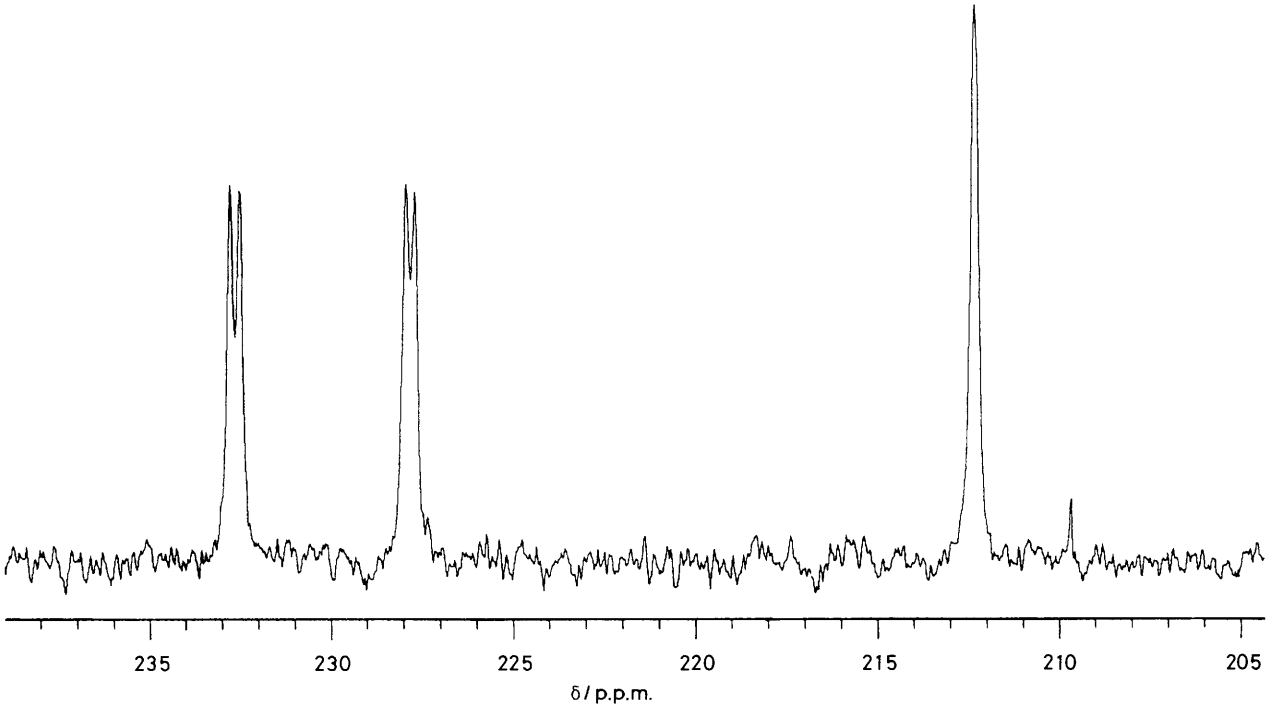

Figure 4. The 100.62-MHz ^{13}C n.m.r. spectrum of the carbonyl ligands of $[Fe_3(CO)_9\{P(OPr^i)_3\}_3]$ at -75 °C in CD_2Cl_2

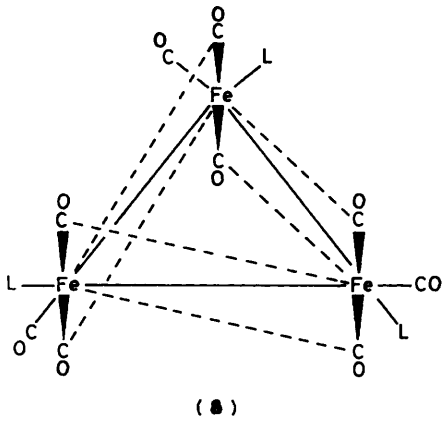

(8)

and 212.5 p.p.m., see Figure 4. At first sight, the structure of (**6**) should give rise to two ^{13}CO n.m.r. signals in the ratio 6:3. However, the *X*-ray structure of $[Fe_3(CO)_{10}\{1,2\text{-}(Me_2As)_2C_6H_4\}]$ shows that even when the ligand constraints prevent a conventionally bridging structure, the carbonyls become semi-bridging.[30] A possible structure for (**7**) which has carbonyls in the ratio 3:3:3 is (**8**). The carbonyls above and below the Fe_3 plane lean in opposite directions. The presence of the $P(OMe)_3$ ligands makes the lean directions of the carbonyls inequivalent, leading to two different chemical shifts for the semi-bridging carbonyls. This type of carbonyl arrangement has been observed in the *X*-ray structure of $[Ru_3(CO)_9(PMe_3)_3]$, but not commented upon.[32] The determination of the Ru···C non-bonding distances for the axial carbonyls shows that exactly the same sort of semi-bridging interaction is occurring, making the axial carbonyls inequivalent in the *X*-ray structure. As iron compounds have a greater tendency to form carbonyl bridges than the corresponding ruthenium compounds, this lean is expected to be more marked in (**7**). These two types of semi-bridging carbonyls have similar chemical shifts, δ 227.8 and 231.3 p.p.m., and $J(^{31}P\text{–}^{13}C)$ values. The equatorial carbonyl at δ 212.5 p.p.m. is in the region found for the equivalent carbonyl C^6 in (**2**) and C^5 in (**5**). A similar dynamic structure with lower symmetry could also give rise to the observed n.m.r. spectrum. The alternative structure (**8**) is considered to be unlikely as it should give rise to ^{13}C n.m.r. signals at *ca.* δ 260, 220, and 210 p.p.m.

The Merry-go-round Mechanism.—The lowest-energy dynamic process which could be studied by n.m.r. spectroscopy in solution is the merry-go-round mechanism, see Scheme 1.

$[Fe_3(CO)_{12}]$. This process has no effect on the ^{13}C n.m.r. spectrum of $[Fe_3(CO)_{12}]$, which is already a singlet as a result of the mechanisms in Scheme 4.

$[Fe_3(CO)_{11}L]$. At −101 °C the ^{13}C n.m.r. spectrum of the carbonyls of $[Fe_3(CO)_{11}\{P(OMe)_3\}]$ consists of three lines in the ratio 5:5:1. The two strong signals exchange, with an activation energy of 8.8 kcal mol^{-1}, presumably *via* the merry-go-round mechanism, leading to two signals with intensities 10:1.

$[Fe_3(CO)_{10}L_2]$. At −92 °C the ^{13}C n.m.r. spectrum of the carbonyls of the major isomer of $[Fe_3(CO)_{10}\{P(OMe)_3\}_2]$, (**2**), is in agreement with this structure. On warming, C^1O, C^2O, C^8O, C^9O, $C^{11}O$, and $C^{12}O$ exchange, with an activation energy of 9.6 kcal mol^{-1}, presumably *via* the merry-go-round mechanism. At −92 °C the ^{13}C n.m.r. spectrum of the minor isomer of $[Fe_3(CO)_{10}\{P(OMe)_3\}_2]$ [**1**; $L^1 = L^2 = P(OMe)_3$], consists of a doublet, $J(^{31}P\text{–}^{13}C) = 13$ Hz. On warming to −40 °C the spectrum is a triplet, $J(^{31}P\text{–}^{13}C) = 7$ Hz. This is consistent with complete scrambling of the carbonyls, presumably *via* the merry-go-round process. No reliable activation energy can be derived due to the small changes involved, but it is about 10 kcal mol^{-1}.

$[Fe_3(CO)_9L_3]$. In the major isomer of $[Fe_3(CO)_9\{P(OMe)_3\}_3]$, (**5**), the merry-go-round mechanism commences at −90 °C, exchanging carbonyls C^1, C^2, C^8, C^9, C^{11}, and C^{12}, with an activation energy of 9.8 kcal mol^{-1}. The mechanism is not possible for the minor isomer of $[Fe_3(CO)_9\{P(OMe)_3\}_3]$, (**7**; R = Me), and the major isomer of $[Fe_3(CO)_9\{P(OPr^i)_3\}_3]$, (**7**; R = Pr^i).

Edge-bridging Carbonyl Exchange.—The next dynamic process involves an edge-bridging intermediate/transition state. This process cannot be observed in $[Fe_3(CO)_{12}]$ or $[Fe_3(CO)_{11}\{P(OMe)_3\}]$ and cannot occur or be observed in the minor isomer of $[Fe_3(CO)_{10}\{P(OMe)_3\}_2]$ [**1**; $L^1 = L^2 = P(OMe)_3$], or the major isomer of $[Fe_3(CO)_{10}\{P(OPr^i)_3\}_2]$ [**1**; $L^1 = L^2 = P(OPr^i)_3$], as the lower-energy dynamic processes have already averaged all the carbonyl ligands. At −50 °C the two inequivalent phosphite ligands in the major isomer of $[Fe_3(CO)_{10}\{P(OMe)_3\}_2]$, (**2**), exchange, with an activation energy of 11.3 kcal mol^{-1}. The ^{13}C n.m.r. spectrum shows that the same time exchange causes broadening of the signals due to carbonyls C^3, C^4, C^6, and C^7. Carbonyls C^3 and C^4 exchange with C^1, C^2, C^8, C^9, C^{11}, and C^{12}, while C^6 and C^7 undergo self-exchange. These observations are consistent with the mechanism in Scheme 5. This mechanism is not possible in the major isomer of $[Fe_3(CO)_9\{P(OMe)_3\}_3]$, (**5**), as it would require an edge-bridging phosphite ligand. A mechanism causes the axial carbonyl ligands in $[Fe_3(CO)_9\{P(OR)_3\}_3]$, (**8**; R = Me or Pr^i), to exchange with an activation energy of 11.5 kcal mol^{-1}, when R = Pr^i. The mechanism in Scheme 5 would cause this exchange, but so would one involving going to a fully terminal carbonyl structure.

Metal-centred Ligand Exchange.—The final dynamic process causes the interconversion of isomers of $[Fe_3(CO)_{10}\{P(OMe)_3\}_2]$, [**1**; $L^1 = L^2 = P(OMe)_3$], with (**2**), and of $[Fe_3(CO)_9\{P(OMe)_3\}_3]$, (**5**), with (**7**) and complete carbonyl scrambling in $[Fe_3(CO)_{11}\{P(OMe)_3\}]$. Most information is available for $[Fe_3(CO)_9\{P(OMe)_3\}_3]$. Magnetization transfer[41,42] has been used fully to analyse the details of the exchange at −33 °C, see Figure 5. The resulting data have been analysed quantitatively as previously described.[42] The analysis shows that the exchange occurs from the $P(OMe)_3$ signal at δ 171.5 to 167.5 p.p.m., with a rate constant of 7.0 s^{-1}, corresponding to $\Delta G^{\ddagger}$ of 13.0 kcal mol^{-1}, and to 163.6 p.p.m., with a rate constant of 8.1 s^{-1}, corresponding to $\Delta G^{\ddagger}$ of 12.9 kcal mol^{-1}. No direct exchange was detected between the $P(OMe)_3$ signal at δ 171.5 p.p.m. to the $P(OMe)_3$ signal at δ 161.8 p.p.m. The $P(OMe)_3$ signals also exchange with the signal due to the other isomer at δ 167.5 p.p.m., at the same rate of 7.0 s^{-1}. In addition, there is exchange between the signals at δ 163.6 and 161.8 p.p.m. with a rate of 5.3 s^{-1}, corresponding to an activation energy of 13.1 kcal mol^{-1}. The probable mechanism involves local exchange at one ion, possibly *via* a trigonal twist, see Scheme 6. As the activation energies for the exchange at each iron atom are approximately the same, the mechanism in Scheme 6 is probably simplified. Rather than complete bridge opening occurring, there is probably concerted bridge opening and closing as the phosphite ligand exchange occurs. It is probably the same mechanism which enables the unique carbonyl to exchange with the other ten carbonyls in $[Fe_3(CO)_{11}\{P(OMe)_3\}]$ with an activation energy of 15.0 kcal mol^{-1} and the interconversion of the isomers of $[Fe_3(CO)_{10}\{P(OMe)_3\}_2]$ with an activation energy of 14.4 kcal mol^{-1}.

The above discussion permits the probable assignment of the ^{31}P n.m.r. signals of $[Fe_3(CO)_{10}\{P(OMe)_3\}_2]$, (**2**), and

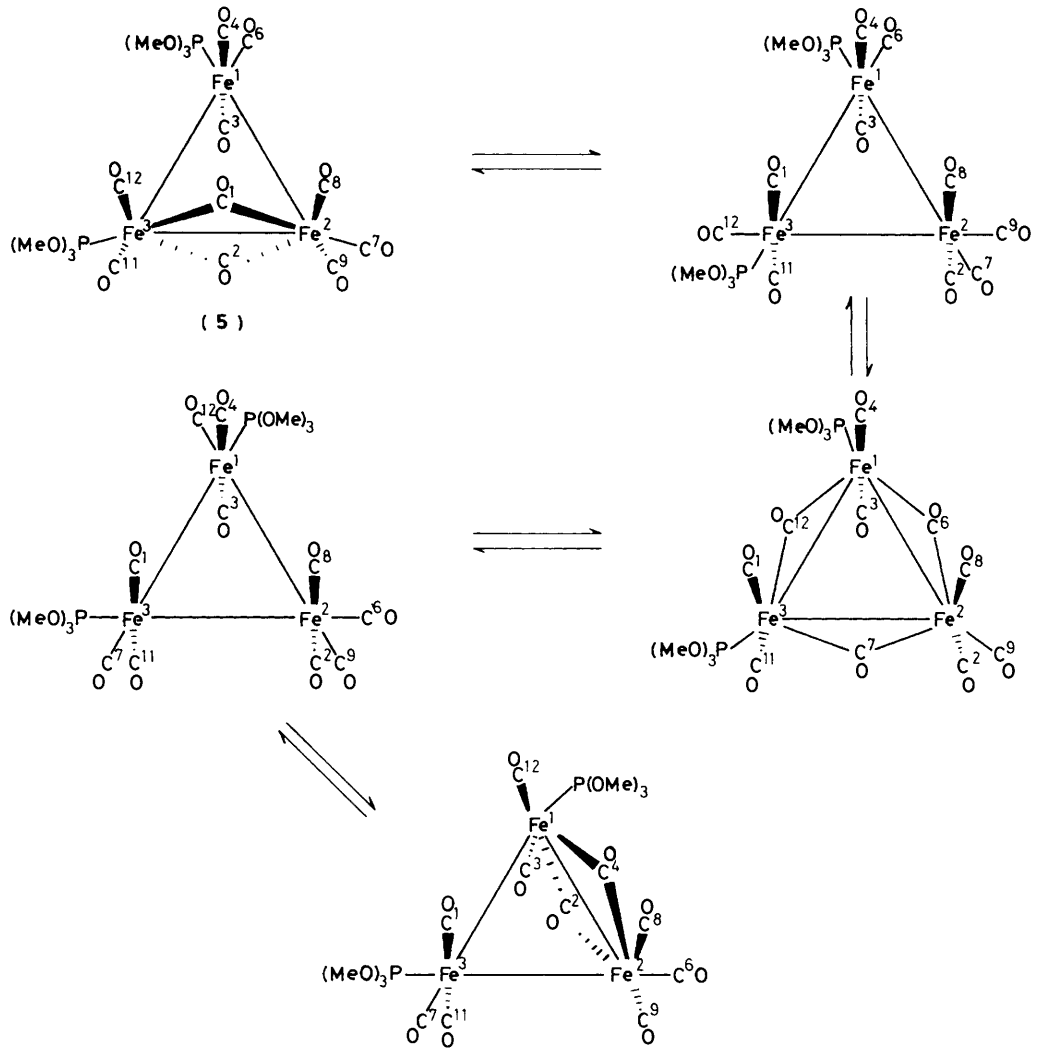

Scheme 5. The proposed mechanism for carbonyl and $P(OMe)_3$ exchange in the unsymmetric isomer of $[Fe_3(CO)_{10}\{P(OMe)_3\}_2]$

$[Fe_3(CO)_9\{P(OMe)_3\}_3]$, (**7**). For $[Fe_3(CO)_9\{P(OMe)_3\}_3]$, (**5**), three ^{31}P signals are observed at δ 171.5, 163.6, and 161.8 p.p.m. The first signal is probably due to the $P(OMe)_3$ on the unbridged Fe^1, the other two signals being due to the $P(OMe)_3$ groups on the bridge Fe^2 and Fe^3. Using the mechanism in Scheme 6, the remaining $P(OMe)_3$ signals may be assigned. Experiment has shown selective magnetization transfer from the $P(OMe)_3$ at δ 171.5 p.p.m. to the $P(OMe)_3$ at δ 163.8 p.p.m. It therefore follows that this $P(OMe)_3$ group is on Fe^3, leaving the signal at δ 161.8 p.p.m. to be assigned to the $P(OMe)_3$ group on Fe^2. The $P(OMe)_3$ ligand on Fe^1 in (**5**) occurs *ca.* 10 p.p.m. to higher frequency than the $P(OMe)_3$ ligand on Fe^3 and this separation is repeated in (**2**), where the signals are at δ 167.4 and 156.7 p.p.m., permitting the assignment of the higher-frequency signal to the $P(OMe)_3$ ligand on Fe^1 and the lower-frequency signal to the one on Fe^3. The highly fluxional isomer, [**1**; L^1 = L^2 = $P(OMe)_3$], has an averaged ^{31}P chemical shift of δ 162.4 p.p.m.

The solution structure of $[Fe_3(CO)_{12}]$ is not directly proven by these experiments. The observation of ^{13}CO signals consistent with the solid-state structure of $[Fe_3(CO)_{12}]$ for $[Fe_3(CO)_{10}\{P(OMe)_3\}_2]$, (**2**), and $[Fe_3(CO)_9\{P(OMe)_3\}_3]$, (**5**), and especially of signals at *ca.* δ 252 p.p.m. has proven the existence of bridging carbonyls in these two compounds at −90 °C in CD_2Cl_2. The dynamic behaviour of $[Fe_3(CO)_{11}\{P(OMe)_3\}]$ is only consistent with this compound existing in CD_2Cl_2 at −101 °C as the bridged species. The dynamic process described in Schemes 2 and 3 give rise to signals in the intensity ratio 5:5:1. Easy access to the unbridged species would lead to the merry-go-round mechanism and at least six carbonyls exchanging. It is probable that the process would occur about both the edges Fe^1–Fe^2 and Fe^2–Fe^3 leading to two signals in the ratio 10:1 as is observed for $[Ru_3(CO)_{11}\{P(OMe)_3\}]$.[43] The same exchange occurs by combining the low-energy mechanisms of Schemes 2 and 3 with a merry-go-round mechanism about either or both edges. The barrier for the merry-go-round mechanism has been measured for $[Fe_3(CO)_{12-n}\{P(OMe)_3\}_n]$ as 8.8 kcal mol^{-1} when n = 1, 9.6 kcal mol^{-1} when n = 2, and 9.8 kcal mol^{-1} when n = 3. It can therefore be estimated that the activation energy for the merry-go-round mechanism in $[Fe_3(CO)_{12}]$ is greater than 7 kcal mol^{-1}. This suggests, but does not prove, that in CD_2Cl_2 at −100 °C $[Fe_3(CO)_{12}]$ is present as the bridged species in agreement with the EXAFS study.[20] There appears to be a strong tendency for these iron compounds to adopt bridging carbonyl structures [13,16,28,29] where possible, and semi-bridging carbonyl structures in other cases.[30] In the case of $[Fe_3(CO)_9\{P(OPr^i)_3\}_3]$, where steric factors prevent the molecule adopting a structure with bridging carbonyls, the molecule adopts a structure with semi-bridging carbonyls, and

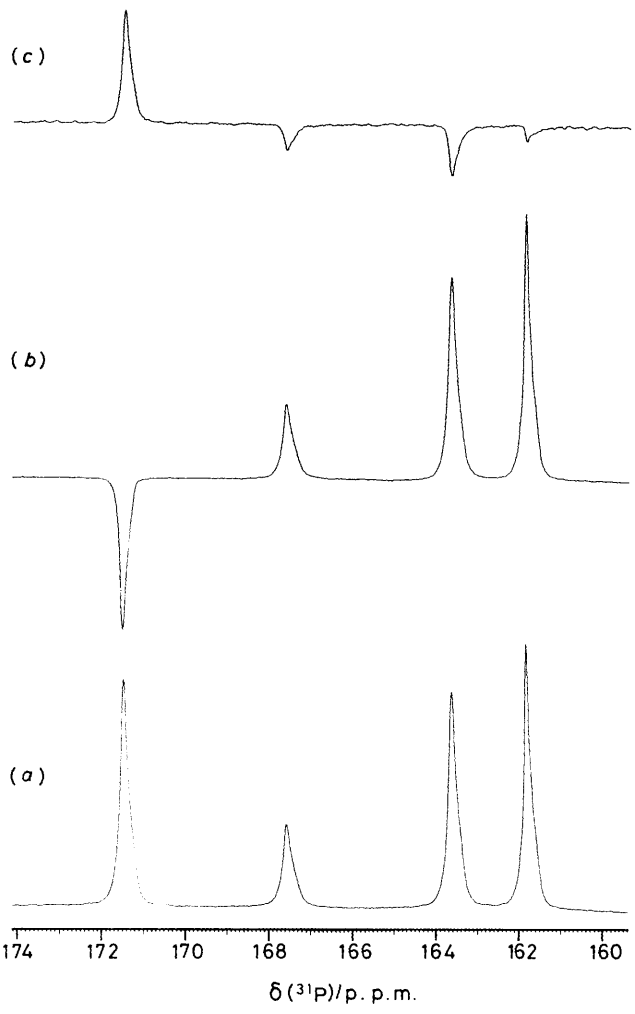

Figure 5. The 162-MHz ^{31}P n.m.r. spectrum of $[Fe_3(CO)_9\{P(OMe)_3\}_3]$ in CD_2Cl_2 at −33 °C. (*a*) The simple spectrum. (*b*) The spectrum after applying a selective π DANTE pulse to the $P(OMe)_3$ signal at δ 171.5 p.p.m. followed immediately by a general $\frac{\pi}{2}$ observing pulse. (*c*) The difference between (*b*) and a similar spectrum with a delay of 10 μs between the selective π DANTE pulse and the general $\frac{\pi}{2}$ observing pulse

the interaction requires an activation energy of 11.5 kcal mol^{-1} to interchange the semi-bridging carbonyls, presumably *via* an unbridged intermediate. It therefore seems probable that $[Fe_3(CO)_{12}]$ and its derivatives prefer to adopt a structure with bridging carbonyls, unless prevented from doing so by steric constraints.

The Solid-state ^{13}C *N.M.R. Spectra of* $[Fe_3(CO)_{12}]$.—The mechanism given in Scheme 2 is also consistent with the solid-state ^{13}C n.m.r. data.[23] The solid-state ^{13}C n.m.r. spectrum of $[Fe_3(CO)_{12}]$ shows signals at δ 238.8, 236.5, 216.0, 209.5, and 198.3 p.p.m. at −93 °C. Hanson suggested that the first two signals arise from the two bridging carbonyls and that the spectrum is consistent with the solid-state structure.[23] Unfortunately, the positions of the signals bear little relation to the values that may be predicted from the chemical shifts in Table 2. In the bridged structure as determined in the solid state, $[Fe_3(CO)_{12}]$ should give signals at approximately δ 252 (C^1O, C^2O), 220 (C^3O, C^4O), 213.5 (C^7O, C^8O, $C^{11}O$, $C^{12}O$), 203.3 (C^9O, $C^{10}O$), and 202.8 p.p.m. (C^5O, C^6O). These values are made more approximate by the lack of a plane of symmetry through the solid-state structure making these approximate signals an average. Nevertheless, a tolerably good match can be achieved with the chemical shifts found in the solid state at −93 °C by assuming that the mechanism given in Scheme 2 is still fast at −93 °C. This gives rise to averaged signals at δ 236, 233, 217, 208, 208, and 203 p.p.m. in good agreement with the solid-state ^{13}C n.m.r. spectrum at −90 °C. The integration of the solid-state ^{13}C n.m.r. spectrum is inconsistent with this conclusion. Hanson *et al.*[23] noted that T_1 at low temperature is very long, in excess of 1 h. Also that the major relaxation mechanism is chemical shift anisotropy. In solution, the same mechanism is dominant,[36–38] and it is then found that bridging carbonyls have considerably longer T_1 values than do terminal carbonyls, and the same is found here for $[Fe_3(CO)_{10}\{P(OMe)_3\}_2]$, (**2**). This difference in relaxation times could lead to inaccurate integrations.

The X-Ray Structure of $[Fe_3(CO)_{10}\{P(OMe)_3\}_2]$.—The molecular structure is illustrated in Figure 6; bond lengths and angles are given in Table 3. The molecule comprises an isosceles triangular array of three iron atoms, with the shortest side [Fe(2)–Fe(3)] bridged by a pair of carbonyls: the geometry of the low-population component Fe_3 triangle is similar, but less well determined. The two triangular arrays are mutually inclined at 33° and interpenetrate so that Fe(1a) and Fe(2a) lie respectively 0.36 and 0.28 Å on one side whilst Fe(3a) lies 0.88 Å on the opposite side of the mean plane through the high-occupancy iron triangle.

Two iron atoms [Fe(1) and Fe(2)] carry equatorial trimethyl phosphite ligands in positions which are both *trans* to the iron–iron bond. The remaining two equatorial sites [on Fe(1) and Fe(3)] are occupied by terminal carbonyl ligands. The two axial carbonyls on Fe(1) seem to be very slightly bent inwards above the Fe_3 triangle, although the effect is marginal and symmetric, favouring neither Fe(2) nor Fe(3). The remaining four terminal carbonyl ligands, two on each of Fe(2) and Fe(3), lie above and below the Fe_3 plane so as to be approximately *trans* to the two bridging carbonyls which link these two iron atoms. An asymmetrically bridging geometry was constrained on these carbon atoms (the oxygen atoms were not constrained) so as to be consistent with previously determined structures of this type. Free refinement had given an unacceptable form of asymmetric bridging with both carbonyls closer to one iron, but the reported structure gave an insignificantly different level of refinement, suggesting that the detailed electron density in this region was ill determined. Since there would be almost total overlap between the unassigned low-occupancy carbonyls associated with the alternative iron core rotamer, and those reported here, some uncertainty in the details of the carbonyl environments would be expected. It is interesting that the sites for the phosphorus atoms are appropriate for both iron environments (again, the effect has been seen before), although the methoxy groups would need different environments. There was some evidence for an alternative set of methoxy oxygen atoms, but it was not convincing and the carbon atoms could not be located; further elaboration of the model was suspended.

Experimental

The n.m.r. spectra in CD_2Cl_2 were measured on a Bruker WH400 spectrometer. The temperatures were measured using a Comark electronic thermometer, by replacing the sample with an n.m.r. tube containing a thermocouple in CH_2Cl_2. Carbon-13 chemical shifts were referenced to the central resonance of CD_2Cl_2 at δ 53.6 p.p.m. Accurate ^{13}C integrals were obtained by using a pulse repetition time in excess of $5T_1$ and without ^1H decoupling. Approximate T_1 values were determined, using the inversion-recovery pulse sequence and a three-parameter fitting program within the Bruker operating system, DISN861 but

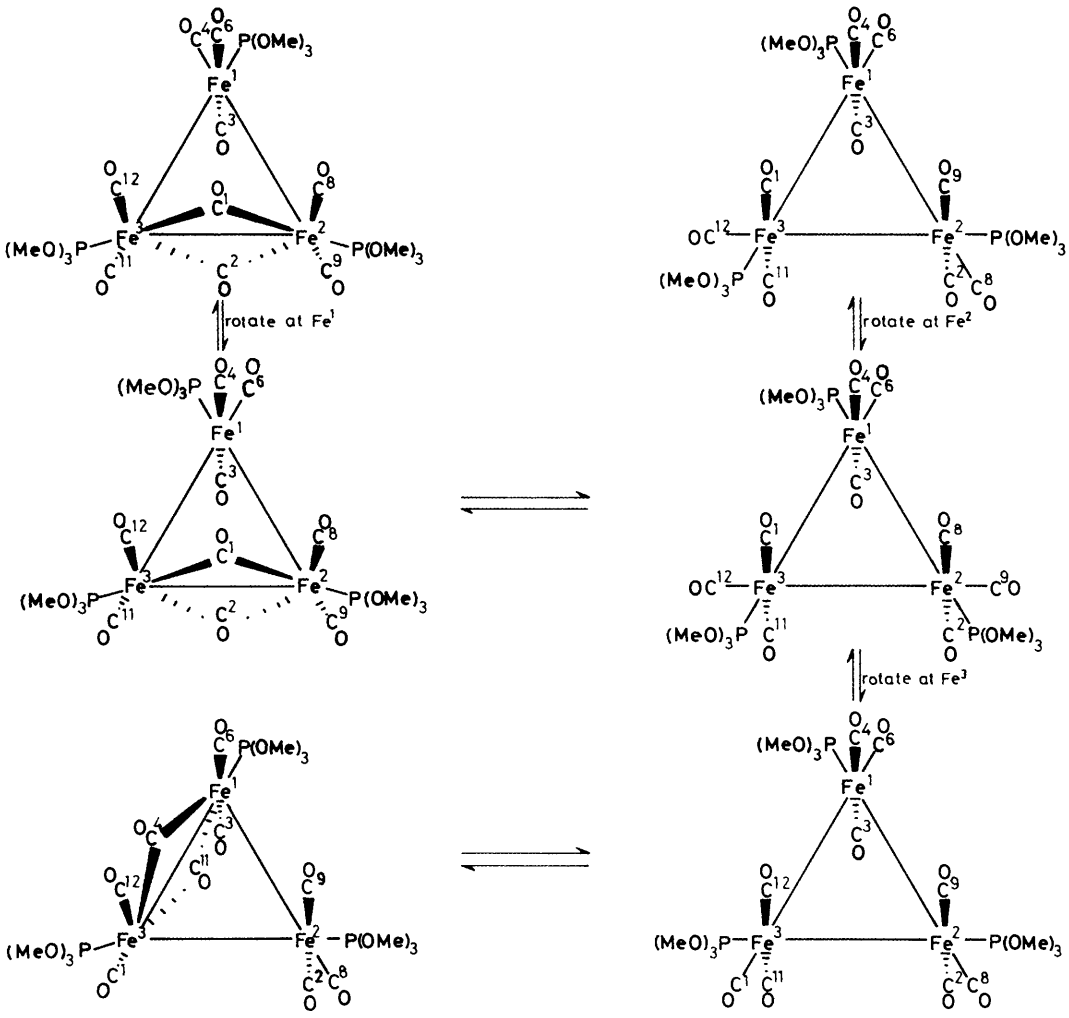

Scheme 6. The proposed mechanism for the interconversion of isomers of $[Fe_3(CO)_9\{P(OMe)_3\}_3]$

with only five delays, 3 μs, 0.05, 0.1, 0.2, and 2, with a 2-s delay between the pulse cycles. Phosphorus-31 chemical shifts were determined relative to external 85% H_3PO_4.

The following experimental procedure was employed to carry out the DANTE[44] measurements. A suitable temperature was chosen so that there was a little line broadening due to exchange. After the spectrometer had stabilized at that temperature, the T_1 values of the $P(OMe)_3$ groups were estimated using the $10D_1$–π–D_1–$\frac{\pi}{2}$ pulse sequence, adjusting the delay, D_1, for null signal. Subsequently, the relaxation delay was taken as $10D_1$. The DANTE pulse length was optimized for maximum signal inversion. The measurements were carried out using the pulse sequence: {[read f.i.d.–{$10D_1$–(D_2 – P_1)$_{30}$–D_3–$\frac{\pi}{2}$–acquire}$_8$–write f.i.d.–change D_3]$_m$–reset exchange delay, D_3}$_n$, with m typically 10, and n chosen to give adequate signal:noise. Typical values are D_1 = 3 s, D_2 = 0.2 ms, P_1 = 2.8 μs, and D_3 = m values with the minimum one being 3 μs and the largest being $10D_1$, and $\frac{\pi}{2}$ pulse = 40.0 μs. The remaining times were chosen to give a spread over the exchange and relaxation times, typically: 0.01, 0.02, 0.04, 0.06, 0.08, 0.1, 0.2, and 0.4 s. This sequence has the advantage that any temperature drift during the experiment will be spread over all the measurements.

The compounds $[Fe_3(CO)_{12}]$,[45] $[Fe_3(CO)_{11}\{P(OMe)_3\}]$,[29] $[Fe_3(CO)_{10}\{P(OMe)_3\}_2]$,[35] and $[Fe_3(CO)_9\{P(OMe)_3\}_3]$[25] were prepared according to the literature methods; $[Fe_3(CO)_{10}\{P(OPr^i)_3\}_2]$ and $[Fe_3(CO)_9\{P(OPr^i)_3\}_3]$ have been previously described,[30] but were synthesized as for the $P(OMe)_3$ analogues.[25]

Crystallography.—Crystal data for $[Fe_3(CO)_{10}\{P(OMe)_3\}_2]$, $C_{16}H_{18}Fe_3O_{16}P_2$, M = 695.77, crystallizes from methanol as dark green needles, which are slightly air-sensitive, crystal dimensions 0.65 × 0.35 × 0.23 mm, monoclinic, a = 10.749(4), b = 21.776(15), c = 11.873(10) Å, β = 109.69(5)°, U = 2 616(3) Å^3, D_c = 1.766 g cm^{-3}, Z = 4, space group $P2_1/n$ (a non-standard setting of $P2_1/c$, C_{2h}^5, no. 14), Mo-K_α radiation ($\bar{\lambda}$ = 0.710 69 Å), μ(Mo-K_α) = 18.31 cm^{-1}, F(000) = 1 399.79.

Three-dimensional, room-temperature X-ray diffraction data were collected in the range 3.5 < 2θ < 50° on a Nicolet R3 diffractometer by the omega scan method. The 2 709 independent reflections for which $|F|/\sigma(|F|) > 3.0$ were corrected for Lorentz and polarization effects, and for absorption by analysis of azimuthal scans. The structure was solved by Patterson and Fourier techniques. The triangular Fe_3 core was found to be disordered over two interpenetrating sites with refined occupancies 0.887 and 0.113; the phosphorus sites were found to be compatible with both iron distributions and were thus included with full occupancy. However, the remaining carbonyl and oxygen sites were applicable only to the major conformer of the core, and were thus included at the appropriate 0.887 population: the light atoms for the minor conformer were not detected and were not included. The $Fe_2(CO)_2$ bridge

Table 3. Bond lengths (Å) and angles (°) in the complex $[Fe_3(CO)_{10}\{P(OMe)_3\}_2]$

Fe(1)–Fe(2)	2.686(4)	Fe(1)–Fe(3)	2.683(3)	P(1)–O(11)	1.530(17)	P(1)–O(12)	1.551(18)
Fe(1)–P(1)	2.184(6)	Fe(1)–C(1)	1.802(15)	P(1)–O(13)	1.470(16)	P(2)–O(14)	1.535(10)
Fe(1)–C(2)	1.814(14)	Fe(1)–C(3)	1.943(20)	P(2)–O(15)	1.540(13)	P(2)–O(16)	1.576(15)
Fe(2)–Fe(3)	2.533(3)	Fe(2)–P(2)	2.166(5)	O(1)–C(1)	1.096(19)	O(2)–C(2)	1.101(18)
Fe(2)–C(4)	1.837(15)	Fe(2)–C(5)	1.814(16)	O(3)–C(3)	0.979(23)	O(4)–C(4)	1.102(18)
Fe(2)–C(6)	1.886(22)	Fe(2)–C(7)	2.090(18)	O(5)–C(5)	1.077(21)	O(6)–C(6)	1.132(24)
Fe(2)–C(6a)	2.089(24)	Fe(2)–C(7a)	1.895(19)	O(6)–C(6a)	1.144(20)	O(7)–C(7)	1.147(16)
Fe(3)–C(6)	2.110(10)	Fe(3)–C(7)	1.908(10)	O(7)–C(7a)	1.137(18)	O(8)–C(8)	1.100(18)
Fe(3)–C(6a)	1.908(12)	Fe(3)–C(7a)	2.103(10)	O(9)–C(9)	1.064(20)	O(10)–C(10)	1.067(20)
Fe(3)–C(8)	1.815(16)	Fe(3)–C(9)	1.810(16)	O(11)–C(11)	1.312(30)	O(12)–C(12)	1.420(32)
Fe(3)–C(10)	1.825(16)	Fe(1a)–Fe(2a)	2.635(27)	O(13)–C(13)	1.322(33)	O(14)–C(14)	1.410(20)
Fe(1a)–Fe(3a)	2.574(21)	Fe(1a)–P(1)	2.239(19)	O(15)–C(15)	1.280(28)	O(16)–C(16)	1.280(20)
Fe(2a)–Fe(3a)	2.520(23)	Fe(2a)–P(2)	2.270(19)				
Fe(2)–Fe(1)–Fe(3)	56.3(1)	Fe(2)–Fe(1)–P(1)	159.7(2)	C(6)–Fe(3)–C(9)	93.0(10)	C(7)–Fe(3)–C(9)	90.3(11)
Fe(3)–Fe(1)–P(1)	103.4(2)	Fe(2)–Fe(1)–C(1)	88.3(5)	C(6a)–Fe(3)–C(9)	86.0(11)	C(7a)–Fe(3)–C(9)	91.5(10)
Fe(3)–Fe(1)–C(1)	86.5(4)	P(1)–Fe(1)–C(1)	91.6(5)	C(8)–Fe(3)–C(9)	97.0(7)	Fe(1)–Fe(3)–C(10)	88.6(5)
Fe(2)–Fe(1)–C(2)	87.3(5)	Fe(3)–Fe(1)–C(2)	87.3(4)	Fe(2)–Fe(3)–C(10)	126.0(4)	C(6)–Fe(3)–C(10)	87.4(7)
P(1)–Fe(1)–C(2)	90.9(5)	C(1)–Fe(1)–C(2)	173.6(6)	C(7)–Fe(3)–C(10)	172.9(12)	C(6a)–Fe(3)–C(10)	83.9(8)
Fe(2)–Fe(1)–C(3)	99.8(6)	Fe(3)–Fe(1)–C(3)	156.0(6)	C(7a)–Fe(3)–C(10)	171.7(9)	C(8)–Fe(3)–C(10)	95.8(7)
P(1)–Fe(1)–C(3)	100.5(6)	C(1)–Fe(1)–C(3)	91.6(7)	C(9)–Fe(3)–C(10)	96.0(7)	Fe(2a)–Fe(1a)–Fe(3a)	57.8(6)
C(2)–Fe(1)–C(3)	93.7(7)	Fe(1)–Fe(2)–Fe(3)	61.8(1)	Fe(2a)–Fe(1a)–P(1)	156.3(7)	Fe(3a)–Fe(1a)–P(1)	98.6(7)
Fe(1)–Fe(2)–P(2)	170.9(1)	Fe(3)–Fe(2)–P(2)	109.1(1)	Fe(1a)–Fe(2a)–Fe(3a)	59.9(7)	Fe(1a)–Fe(2a)–P(2)	165.0(8)
Fe(1)–Fe(2)–C(4)	86.4(6)	Fe(3)–Fe(2)–C(4)	126.0(6)	Fe(3a)–Fe(2a)–P(2)	105.4(7)	Fe(1a)–Fe(3a)–Fe(2a)	62.3(7)
P(2)–Fe(2)–C(4)	99.6(6)	Fe(1)–Fe(2)–C(5)	87.4(5)	Fe(1)–P(1)–O(11)	114.2(10)	Fe(1)–P(1)–O(12)	116.6(7)
Fe(3)–Fe(2)–C(5)	126.6(5)	P(2)–Fe(2)–C(5)	99.3(6)	O(11)–P(1)–O(12)	95.3(11)	Fe(1)–P(1)–O(13)	117.4(8)
C(4)–Fe(2)–C(5)	90.7(7)	Fe(1)–Fe(2)–C(6)	85.5(8)	O(11)–P(1)–O(13)	104.0(11)	O(12)–P(1)–O(13)	106.5(11)
P(2)–Fe(2)–C(6)	88.6(9)	C(4)–Fe(2)–C(6)	82.4(8)	Fe(2)–P(2)–O(14)	112.4(5)	Fe(2)–P(2)–O(15)	121.5(8)
C(5)–Fe(2)–C(6)	170.3(10)	Fe(1)–Fe(2)–C(7)	82.1(8)	O(14)–P(2)–O(15)	105.1(7)	Fe(2)–P(2)–O(16)	116.6(7)
P(2)–Fe(2)–C(7)	91.9(8)	C(4)–Fe(2)–C(7)	168.5(10)	O(14)–P(2)–O(16)	100.1(8)	O(15)–P(2)–O(16)	98.2(10)
C(5)–Fe(2)–C(7)	88.5(7)	C(6)–Fe(2)–C(7)	97.0(7)	P(1)–O(11)–C(11)	134.7(23)	P(1)–O(12)–C(12)	122.3(15)
Fe(1)–Fe(2)–C(6a)	85.2(7)	P(2)–Fe(2)–C(6a)	87.9(8)	P(1)–O(13)–C(13)	131.9(19)	P(2)–O(14)–C(14)	126.6(10)
C(4)–Fe(2)–C(6a)	90.6(8)	C(5)–Fe(2)–C(6a)	172.4(8)	P(2)–O(15)–C(15)	133.6(19)	P(2)–O(16)–C(16)	134.5(16)
Fe(1)–Fe(2)–C(7a)	87.5(8)	P(2)–Fe(2)–C(7a)	87.2(9)	Fe(1)–C(1)–O(1)	173.0(16)	Fe(1)–C(2)–O(2)	174.6(13)
C(4)–Fe(2)–C(7a)	172.0(12)	C(5)–Fe(2)–C(7a)	84.0(8)	Fe(1)–C(3)–O(3)	177.6(22)	Fe(2)–C(4)–O(4)	178.7(14)
C(6a)–Fe(2)–C(7a)	93.9(7)	Fe(1)–Fe(3)–Fe(2)	61.9(1)	Fe(2)–C(5)–O(5)	179.5(12)	Fe(2)–C(6)–Fe(3)	78.5(6)
Fe(1)–Fe(3)–C(6)	81.5(9)	Fe(1)–Fe(3)–C(7)	85.5(10)	Fe(2)–C(6)–O(6)	149.9(11)	Fe(3)–C(6)–O(6)	130.9(15)
C(6)–Fe(3)–C(7)	95.7(7)	Fe(1)–Fe(3)–C(6a)	88.8(10)	Fe(2)–C(7)–Fe(3)	78.5(5)	Fe(2)–C(7)–O(7)	128.0(11)
Fe(1)–Fe(3)–C(7a)	83.6(9)	C(6a)–Fe(3)–C(7a)	93.1(8)	Fe(3)–C(7)–O(7)	153.1(17)	Fe(2)–C(6a)–Fe(3)	78.5(8)
Fe(1)–Fe(3)–C(8)	88.2(5)	Fe(2)–Fe(3)–C(8)	124.6(5)	Fe(2)–C(6a)–O(6)	126.8(12)	Fe(3)–C(6a)–O(6)	153.6(16)
C(6)–Fe(3)–C(8)	169.1(10)	C(7)–Fe(3)–C(8)	80.1(7)	Fe(2)–C(7a)–Fe(3)	78.4(5)	Fe(2)–C(7a)–O(7)	150.4(11)
C(6a)–Fe(3)–C(8)	177.0(11)	C(7a)–Fe(3)–C(8)	86.9(7)	Fe(3)–C(7a)–O(7)	131.1(14)	Fe(3)–C(8)–O(8)	171.4(14)
Fe(1)–Fe(3)–C(9)	172.6(5)	Fe(2)–Fe(3)–C(9)	110.8(5)	Fe(3)–C(9)–O(9)	175.4(17)	Fe(3)–C(10)–O(10)	172.4(16)

Table 4. Atom co-ordinates ($\times 10^4$)

Atom	*x*	*y*	*z*	Atom	*x*	*y*	*z*
Fe(1)	3 851(2)	1 418(1)	894(2)	O(14)	2 224(11)	526(5)	4 510(8)
Fe(2)	2 480(2)	785(1)	2 027(2)	O(15)	1 365(18)	−347(5)	3 192(13)
Fe(3)	4 305(2)	1 493(1)	3 255(2)	O(16)	101(12)	553(8)	3 024(14)
Fe(1a)	4 783(16)	1 532(8)	2 036(14)	C(1)	2 710(15)	2 044(7)	739(11)
Fe(2a)	3 247(16)	893(8)	2 926(15)	C(2)	5 008(13)	782(7)	1 222(11)
Fe(3a)	2 337(16)	1 322(7)	835(14)	C(3)	2 940(17)	1 151(8)	−739(19)
P(1)	5 335(5)	2 030(2)	623(4)	C(4)	993(16)	1 017(8)	795(16)
P(2)	1 562(4)	353(2)	3 192(3)	C(5)	2 669(14)	117(7)	1 188(12)
O(1)	2 075(11)	2 451(5)	575(11)	C(6)	2 225(10)	1 553(9)	2 654(27)
O(2)	5 697(11)	394(5)	1 330(10)	C(7)	4 374(17)	617(4)	3 237(28)
O(3)	2 507(16)	1 028(8)	−1 573(11)	C(6a)	2 456(10)	1 610(9)	2 919(27)
O(4)	88(12)	1 147(7)	60(12)	C(7a)	4 125(18)	531(4)	3 133(27)
O(5)	2 774(13)	−283(6)	692(10)	C(8)	6 049(15)	1 382(7)	3 491(12)
O(6)	1 547(11)	1 897(5)	2 868(11)	C(9)	4 431(16)	1 478(7)	4 814(13)
O(7)	4 849(9)	152(5)	3 589(9)	C(10)	4 332(15)	2 327(7)	3 127(13)
O(8)	7 126(10)	1 316(6)	3 778(10)	C(11)	5 407(25)	3 227(9)	399(24)
O(9)	4 550(13)	1 503(7)	5 739(10)	C(12)	5 778(27)	1 647(10)	−1 283(21)
O(10)	4 332(15)	2 817(5)	3 165(11)	C(13)	7 813(24)	2 235(13)	1 478(28)
O(11)	5 113(21)	2 710(7)	819(19)	C(14)	1 949(15)	292(7)	5 499(12)
O(12)	5 310(16)	2 109(8)	−682(13)	C(15)	2 082(25)	−807(9)	3 135(19)
O(13)	6 721(16)	1 923(9)	1 359(17)	C(16)	−1 018(17)	476(10)	2 201(16)

Atoms Fe(1a), Fe(2a), and Fe(3a) comprise the low-occupancy (0.113) iron core, C(6), C(7), C(6a), and C(7a) the disordered bridging carbonyl ligands, each with occupancy 0.50. All other atoms have occupancy 0.887, except for P(1) and P(2) which have full occupancy.

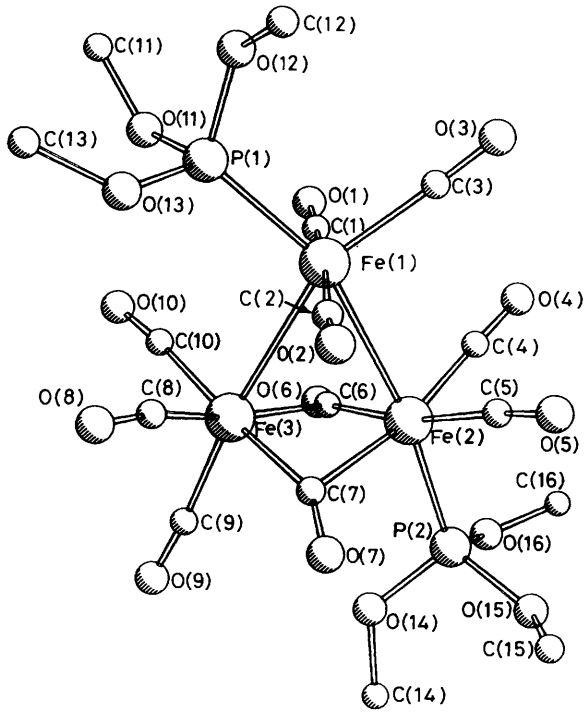

Figure 6. The *X*-ray structure of one isomer of $[Fe_3(CO)_{10}\{P(OMe)_3\}_2]$

fragment refined with an unacceptable geometry and a similar, disordered asymmetric bridge to that reported for related molecules was constrained during refinement by blocked-cascade least-squares methods. Hydrogen atoms were placed in calculated positions with isotropic thermal parameters related to those of the supporting carbon atoms. Refinement converged at a final *R* 0.0944 with allowance for the anisotropic thermal vibrations of all non-hydrogen atoms, with the exception of the carbon atoms of the disordered bridging carbonyls. Complex scattering factors were taken from the program package SHELXTL[46] which was used for the refinement, during which unit weights were used. Table 4 lists atomic positions.

Additional material available from the Cambridge Crystallographic Data Centre comprises H-atom co-ordinates and thermal parameters.

Acknowledgements

We thank the S.E.R.C. for financial support and the Staffordshire County Council for a maintenance grant (to G. W. B.).

References

1 J. Dewar and H. O. Jones, *Proc. R. Soc. London, Ser.* A, 1906, **79**, 66.
2 C. H. Wei and L. F. Dahl, *J. Am. Chem. Soc.*, 1969, **91**, 1351.
3 W. Hieber and E. Becker, *Chem. Ber.*, 1930, **63**, 1405.
4 R. K. Sheline, *J. Am. Chem. Soc.*, 1951, **73**, 1615.
5 J. W. Cable and R. K. Sheline, *Chem. Rev.*, 1956, **56**, 1.
6 F. A. Cotton and G. Wilkinson, *J. Am. Chem. Soc.*, 1957, **79**, 752.
7 K. Noack, *Helv. Chim. Acta*, 1962, **4**, 1847.
8 G. R. Dobson and R. K. Sheline, *Inorg. Chem.*, 1963, **2**, 1313.
9 M. Kalvius, U. Zahn, P. Kienle, and H. Eicher, *Z. Naturforsch., Teil. A*, 1962, **17**, 494.
10 E. Fluck, W. Kerler, and W. Neuwirth, *Angew. Chem., Int. Ed. Engl.*, 1963, **2**, 277.
11 R. H. Herber, W. R. Kingston, and G. K. Wertheim, *Inorg. Chem.*, 1963, **2**, 1313.
12 L. F. Dahl and J. F. Blount, *Inorg. Chem.*, 1965, **4**, 1373.
13 D. J. Dahm and R. A. Jacobsen, *Chem. Commun.*, 1966, 496; *J. Am. Chem. Soc.*, 1968, **90**, 5106.
14 E. R. Corey and L. F. Dahl, *Inorg. Chem.*, 1962, **1**, 521.
15 C. H. Wei and L. F. Dahl, *J. Am. Chem. Soc.*, 1966, **88**, 1821.
16 F. A. Cotton and J. M. Troup, *J. Am. Chem. Soc.*, 1974, **95**, 4155.
17 M. R. Churchill, F. J. Hollander, and J. P. Hutchinson, *Inorg. Chem.*, 1977, **16**, 2655.
18 M. Poliakoff and J. J. Turner, *Chem. Commun.*, 1970, 1008.
19 S. Dobbs, S. Nunziante-Cesaro, and M. Maltese, *Inorg. Chim. Acta*, 1986, **113**, 167.
20 N. Binsted, J. Evans, G. N. Graves, and R. J. Price, *J. Chem. Soc., Chem. Commun.*, 1987, 1330.
21 F. A. Cotton and D. L. Hunter, *Inorg. Chim. Acta*, 1974, **11**, L9.
22 H. Dorn, B. E. Hanson, and E. Motell, *Inorg. Chim. Acta*, 1981, **54**, L71.
23 B. E. Hanson, C. Lisic, J. T. Petty, and G. A. Iannaconne, *Inorg. Chem.*, 1986, **25**, 4062.
24 R. E. Benfield, P. D. Gavens, B. F. G. Johnson, M. J. Mays, S. Aime, L. Milone, and D. Ostella, *J. Chem. Soc., Dalton Trans.*, 1981, 1535.
25 D. H. Farrar and J. A. Lunniss, *J. Chem. Soc., Dalton Trans.*, 1987, 1249.
26 H. B. Burgi and J. D. Dunitz, *Acc. Chem. Res.*, 1983, **16**, 153.
27 D. Braga and B. T. Heaton, *J. Chem. Soc., Chem. Commun.*, 1987, 608.
28 M. I. Bruce, T. W. Hambley, and B. K. Nicholson, *J. Chem. Soc., Dalton Trans.*, 1983, 2385.
29 W. S. McDonald, J. R. Moss, G. Raper, B. L. Shaw, R. Greatrex, and N. N. Greenwood, *Chem. Commun.*, 1969, 1295; G. Raper and W. S. McDonald, *J. Chem. Soc. A*, 1971, 3430.
30 A. Bino, F. A. Cotton, P. Lahuerta, P. Puebla, and R. Uson, *Inorg. Chem.*, 1980, **19**, 2357.
31 M. I. Bruce, D. Schultz, R. C. Wallis, and A. D. Redhouse, *J. Organomet. Chem.*, 1979, **169**, C15; M. I. Bruce, J. G. Matisons, J. M. Patrick, A. H. White, and A. C. Willis, *J. Chem. Soc., Dalton Trans.*, 1985, 1223; E. J. Forbes, N. Goodhand, D. L. Jones, and T. A. Hamor, *J. Organomet. Chem.*, 1979, **182**, 143; P. J. Roberts and J. Trotter, *J. Chem. Soc. A*, 1971, 1479.
32 M. I. Bruce, J. G. Matisons, B. W. Skelton, and A. H. White, *J. Chem. Soc., Dalton Trans.*, 1983, 2375.
33 J. J. de Boer, J. A. van Doorn, and C. Masters, *J. Chem. Soc., Chem. Commun.*, 1978, 1005.
34 A. Forster, B. F. G. Johnson, J. Lewis, T. W. Matheson, B. H. Robinson, and W. G. Jackson, *J. Chem. Soc., Chem. Commun.*, 1974, 1042; B. F. G. Johnson, J. Lewis, B. E. Reichert, and K. T. Schorpp, *J. Chem. Soc., Dalton Trans.*, 1976, 1403; R. F. Alex and R. K. Pomeroy, *Organometallics*, 1987, **6**, 2437; *J. Organomet. Chem.*, 1985, **284**, 379; A. J. Deeming, S. Donovan-Mtunzi, and S. E. Kabir, *ibid.*, **281**, C43.
35 P. J. Pollick and A. Wojcicki, *J. Organomet. Chem.*, 1968, **14**, 469.
36 G. E. Hawkes, E. W. Randall, S. Aime, and R. Gobetto, *J. Magn. Reson.*, 1986, **68**, 597.
37 B. E. Mann, B. T. Pickup, and A. K. Smith, *J. Chem. Soc., Dalton Trans.*, 1989, 889.
38 S. Aime, M. Botta, R. Gobetta, and D. Ostella, *J. Chem. Soc., Dalton Trans.*, 1988, 791.
39 See for example, B. E. Mann and B. F. Taylor, '^{13}C N.M.R. Data for Organometallic Compounds,' Academic Press, London, 1981.
40 S. M. Grant and A. R. Manning, *Inorg. Chim. Acta*, 1978, **31**, 41.
41 S. Forsén and R. A. Hoffman, *J. Chem. Phys.*, 1963, **39**, 2892; R. A. Hoffmann and S. Forsén, *Prog. Nucl. Magn. Reson. Spectrosc.*, 1966, **1**, 171.
42 M. Grassi, B. E. Mann, B. T. Pickup, and C. M. Spencer, *J. Magn. Reson.*, 1986, **69**, 92.
43 G. W. Bentley and B. E. Mann, unpublished work.
44 G. A. Morris and R. Freeman, *J. Magn. Reson.*, 1978, **29**, 433.
45 W. McFarlane and G. Wilkinson, *Inorg. Synth.*, 1966, **8**, 181.
46 G. M. Sheldrick, SHELXTL System for Crystal Structure Solution, University of Göttingen, 1983, revision 4.

Received 18*th July* 1988; *Paper* 8/02880J